

Impact of plasma concentration of transferrin on targeting capacity of nanoparticles

Mohammad Reza Sepand^a, Mahdi Ghavami^b, Steven Zanganeh^c, Sabrina Stacks^d, Forough Ghasemi^e, Hamed Montazeri^f, Claudia Corbo^{g,h}, Hossein Derakhshankhahⁱ, Seyed Nasser Ostad^a, Mohammad Hossein Ghahremani^{a*} and Morteza Mahmoudi^{j*}

^aDepartment of Toxicology and Pharmacology, Faculty of Pharmacy, Tehran University of Medical Sciences, Tehran, Iran

^bDepartment of Cellular and Molecular Medicine, University of Copenhagen, Blegdamsvej 3, DK-2200 Copenhagen N, Denmark

^cSloan Kettering Institute for Cancer Research, 1275 York Avenue, New York, NY 10065, United States

^dVassar College address 124 Raymond Ave, Poughkeepsie, NY 12604, United States

^eDepartment of Nanotechnology, Agricultural Biotechnology Research Institute of Iran (ABRII), Agricultural Research, Education, and Extension Organization (AREEO), Karaj, Iran.

^fSchool of Pharmacy-International Campus, Iran University of Medical Sciences, Tehran, Iran

^gSchool of Medicine and Surgery, University of Milano-Bicocca, Monza, Italy

^hNanomedicine Center NANOMIB, University of Milano-Bicocca, Milano, Italy

ⁱPharmaceutical Sciences Research Center, Health Institute, Kermanshah University of Medical Sciences, Kermanshah, Iran.

^jDepartment of Radiology and Precision Health Program, MI 48824, United States

*Corresponding authors: mhghahremani@tums.ac.ir; mahmou22@msu.edu

Supplemental Methods

Preparation of gold seeds

For the preparation of gold seeds, 250 μL of aqueous $\text{HAuCl}_4 \cdot 3\text{H}_2\text{O}$ (0.01 mol L^{-1}) was added to 10 mL of a CTAB solution (0.10 mol L^{-1}) in a glass test tube, and mixed by gentle stirring until the color of the mix solution turned bright brown-yellow. Then, 500 μL of the aqueous ice-cold NaBH_4 solution (0.01 mol L^{-1}) was added and mixed for 10 min. In this stage, the color changed to pale brown-yellow. The seeds were kept at $25 \text{ }^\circ\text{C}$ until the next step.

Preparation of gold nanospheres

In order to synthesize 20 nm gold nanospheres, 50 μL of freshly prepared 0.1 mol L^{-1} water-soluble ascorbic acid solution was added to 7.5 mL of growth solution containing 45 mL of CTAB (0.1 mol L^{-1}) and 500 μL of HAuCl_4 (0.01 M). Then, the mixture was stirred with 2.5 mL of seed solution for 10 min to reach the wine red solution of gold nanospheres with a diameter of 20 nm.¹

Preparation of gold nanorods

For the preparation of gold nanorods, a mixture of 50 μL of silver nitrate solution (0.01 mol L^{-1}) and 5 mL of CTAB (0.10 mol L^{-1}) was prepared at $25 \text{ }^\circ\text{C}$. Then, the solution was mixed gently after adding 250 μL of HAuCl_4 (0.01 mol L^{-1}). Finally, 30 μL of ascorbic acid (0.1 mol L^{-1}), as a mild reducing agent, was added to the solution. The color of the growth solution was changed from dark yellow to colorless after the addition of ascorbic acid. Finally, 12 μL of the seed solution was added to the growth solution at $27\text{--}30 \text{ }^\circ\text{C}$. This process produced pure nanorods solution with an aspect ratio of 4.¹

In order to remove excess CTAB, the gold nanospheres were washed three times with deionized water (DI) followed by 20 min centrifugation at 15000 g. For gold nanorods purification, NPs were washed three times with DI water and centrifuged for 10 min at 10000 g while avoiding the nanorods aggregation.¹

Surface modification of gold nanoparticles

The surface of CTAB capped gold nanostructures was modified with HS-PEG-NH₂ using a ligand exchange method. Briefly, 1.2 mL of an aqueous solution of HS-PEG-NH₂ (0.25 mmol L^{-1}) was mixed with 3 mL of aqueous suspension of gold nanostructures (1.7 nmol L^{-1}), and then DI water was added to the final volume of 6.0 mL. The final concentration of Au NPs and HS-PEG-NH₂ were 0.85 nmol L^{-1} and $50 \text{ } \mu\text{mol L}^{-1}$, respectively. The reaction solution was mixed gently prior to overnight incubation at $4 \text{ }^\circ\text{C}$ followed by centrifugation at 14000 rpm for 5 min. The supernatant was

carefully collected and the solution was centrifuged two more times to remove the remaining Au NPs.² The Au NPs were decorated with HS-PEG2000-NH₂ through covalent gold-thiol linkages which reduces nonspecific interactions and facilitates high specific interaction between targeting ligands and cell surface receptors.³

Finally, 0.25 mL of FITC-labeled transferrin (Tf) (1 mg mL⁻¹) was added to 0.25 mL of the PEG-NPs solution. The PEG and Tf-conjugated Au NPs (Tf-PEG-NPs) were formed by the reaction between the protein's amino groups and NH₂-PEG molecules which make stable amide bonds.⁴

Protein-nanoparticle interactions by UV-Vis spectroscopy

UV-vis absorption is a simple method for protein-nanoparticle interactions assessment.⁵ The UV-vis spectra of the Transferrin (Tf) and PEGylated Gold Nanorods (PEG-Au NRs) complex were measured with a Cary spectrophotometer, 100 Bio-model, with jacketed cell holders. UV-vis spectroscopy of Tf protein (0.75 mg mL⁻¹) was measured in the presence and absence of increasing concentrations of PEGylated Au NRs (50-100 mg mL⁻¹).

Interaction of Transferrin with PEGylated Au NRs.

The fluorescence quenching is a very useful tool which provides much information about protein-nanoparticle interactions in molecular levels.⁶ In addition, the binding information between nanoparticles and proteins, such as binding sites and binding affinity (Gibbs free energy (ΔG)) can be revealed by this technique.⁷

Transferrin quenching behavior in contact with PEGylated Au NRs.

In order to determine the molecular quenching mechanism, the fluorescence quenching results were analyzed by Stern-Volmer equation. Determination of quenching rate constants is a good criterion for mechanism detection. Thus, the Stern-Volmer equation was used to determine the fluorescence quenching mechanism⁸:

$$F_0/F = 1 + K_{SV} [Q] = 1 + K_q \tau [Q]$$

F_0 and F reveal the fluorescence intensities at steady-state of Transferrin in the absence and presence of different concentrations of PEG-Au NRs. K_{SV} is the Stern-Volmer quenching constant and is gained from linear regression of Stern-Volmer equation; K_q is the quenching rate constant of protein whose maximum value is known to be $2.0 \times 10^{10} \text{ L mol}^{-1} \text{ s}^{-1}$.⁹ $[Q]$ is the concentration of quencher (PEG-Au NRs). τ is the average lifetime of the fluorophore/ biomacromolecule in the absence of the quencher.

Binding sites analysis

The following double–logarithm equation provides more information about binding equilibrium:

$$\text{Log } ((F_0-F)/F) = \text{Log } K + n\text{Log } [Q]$$

In this equation, n is the number of binding sites per protein and $K\alpha$ is the association constant.

Thermodynamic analysis

Obtaining the thermodynamic parameters of protein-ligand interaction is the best way for determining the interaction type and affinity.

Free energy changes of the interaction between Transferrin and the nanoparticles can be obtained from the following formula for each temperature ¹⁰:

$$\Delta G = -RT\ln K$$

In this equation, K is the association/binding constants for PEG-Au NRs; T is the temperature of experiments and R is the gas constant ($8.314 \text{ J mol}^{-1} \text{ K}^{-1}$).

The ΔG was calculated from Gibbs equation and other parameters can be obtained by plotting the binding and quenching constants according to van't Hoff equation ¹⁰:

$$\ln K = - (\Delta H/RT) + (\Delta S/R)$$

Plasma preparation

Blood samples from healthy volunteers and patients were collected in citrate coated tubes and prepared based on HUPO guidelines¹¹ with signed consent information by ethical laws. After 5 min centrifugation of the citrated tube at 2500 g at 4 °C, the supernatant was removed. Aliquots of samples were stored in 1.5 mL tubes at $-20 \text{ }^\circ\text{C}$ to avoid thaw and freezing.

Physical characterization of protein–corona

Dynamic Light Scattering (DLS, Malvern Instruments, Worcestershire, UK) and a Zetasizer (Malvern Instruments, Worcestershire, UK) equipped with a light source of wavelength 532 nm were used to determine the size and surface charge of Au NPs. The NPs solutions (0.8 mL) were analyzed for the refractive index, the absorption coefficient of the Au NPs material and solvent viscosity for each NP type. Each data was the average of at least five independent measurements.

Immuno-blot detection of Tf after binding to PEGylated Au NPs.

Immuno-blot detection of pegylated Au NPs conjugated with human Tf or albumin (Tf-PEG-Au NPs and albumin-PEG-Au NPs, respectively), and the corresponding pegylated precursor (PEG-Au NPs). Dot blots were prepared by spotting human Tf antibody (Abcam-ab82411) on nitrocellulose membranes. Primary antibody (1 μL of 100 $\mu\text{g mL}^{-1}$) is spotted on the membranes, which were then exposed to the different nanoparticles (40 $\mu\text{g mL}^{-1}$ in PBS). The fluorescence signal of the nanoparticles was detected in the cases where the Au NPs binded to the antibody on the dot blot.

Preparation and characterization of Tf depleted human plasma

Protein plasma with 100 mg mL^{-1} concentration was estimated using a BCA commercial kit and applied for further investigation. In order to deplete endogenous transferrin from human plasma, immunoprecipitation (IP) assay was carried out using IP kit (Sigma-Aldrich, St. Louis, MO, USA). Briefly, 50 μL of rabbit polyclonal antibody against human Tf (Abcam-ab82411) was added to a microtube containing 10 μL of human plasma and incubated for 2 h at 37 $^{\circ}\text{C}$ with slow shaking. Following the incubation, 30 μL of protein G agarose was added to the mixture and incubated for another 2 h, at room temperature with slow shaking. Finally, the tube was centrifuged at 13000 g for 30 min and the supernatant was collected carefully. The pellet contained the Tf bound to antibody and protein G agarose. The supernatant was subjected to another centrifugation with the same condition for further depletion, and supernatant solution was considered as human depleted transferrin. To confirm the Tf depletion, we performed western blot analysis for Tf and further silver nitrate staining on samples. These assessments showed that the overall pattern of plasma was conserved (except Tf level), no aggregates were formed and plasma protein dispersion was not affected by the depletion process and the sample concentration.

Cell culture and treatments

HT29 (Human colorectal adenocarcinoma, epithelial-like cell line) cells were purchased from the Pasteur Institute (Iran) and cultured in RPMI medium (Biosera, Austria) supplemented with 10% fetal bovine serum (FBS) (Gibco, USA) and 1% penicillin/streptomycin (Biowest, France) in a 37 $^{\circ}\text{C}$ humidified atmosphere of 5%. OVCAR3 (human ovarian carcinoma cell line) cells were purchased from the Pasteur Institute (Iran) and cultured in high glucose DMEM (Biosera, Austria) medium supplemented with 10% FBS (Gibco, USA), and 1% penicillin/streptomycin (Biowest, France). HT29 and OVCAR3 were sub-cultured after reaching 70% confluency with trypsin-EDTA (Gibco, USA) and seeded with fresh medium.

Lactate dehydrogenase release assessment

LDH release in media was used as cells membrane damage indicator by a LDH kit purchased from Cayman (Cayman, 601170). Briefly, cells were incubated with Au NPs test media ($5\text{-}40\ \mu\text{g mL}^{-1}$) for 6 h in the 96-well plate at $37\ ^\circ\text{C}$, $5\ \%$ CO_2 . Following incubation, supernatant media ($100\ \mu\text{L}$) was transferred into new 96 well plate and kept with LDH reaction solution ($100\ \mu\text{L}$) (NAD^+ , lactic acid, diaphorase and INT) for 30 min at room temperature. Lastly, the absorbance was read at $490\ \text{nm}$ by BioTek microplate reader.

Design and synthesis of siRNA and transfection procedure

For TFRC RNAi, double-stranded siRNA were designed according to Elbashir *et al.* method¹² in a way to be common in both variants of transferrin receptor 2 (NM_003227.3 and NM_001206855.1) and were synthesized by Eurofins MWG Operon (Germany). The sequence of siRNA is as follows: sense, $5'\text{-GCTCAAGGAGTGCTCATATdTdT-3}'$; and, anti-sense $5'\text{-dTdTTTATACTCGTGAGGAACTCG-3}'$. SiRNA was dissolved in 1X siMAX universal buffer ($6\ \text{mmol L}^{-1}$ HEPES, $20\ \text{mmol L}^{-1}$ KCl, $0.2\ \text{mmol L}^{-1}$ MgCl_2 ; pH 7.3; sterile). Scrambled siRNA with no significant homology to any known human transcript was also administered as a control.

HT29 and OVCAR3 cells were plated at a density of approximately 10,000 cells per well in 6-well-plate culture dishes, supplemented with 10% FBS without antibiotic and permitted to attach for 24 h. SiRNA transfection was carried out according to the manufacturer's protocol using Lipofectamine 2000 (Invitrogen, USA). Briefly, either 40 pmol (in case of HT29 cells) or 30 pmol (in case of OVCAR-3 cells) of SiRNA was added to $200\ \mu\text{L}$ of opti-MEM (Gibco, USA). The Lipofectamine 2000 ($10\ \mu\text{L}$) was mixed with $200\ \mu\text{L}$ of opti-MEM and kept at ambient temperature for 15 min. These solutions were then mixed and further incubated for 30 min at room temperature. Final $400\ \mu\text{L}$ mixture was added to each well of the 6-well plate and replaced with a regular medium after six hours. The cells were cultured for an additional 72 h prior to TFRC expression analysis by western blotting.

Western blot of samples

For detection of Tf in depleted samples, the supernatant from depleted plasma was subjected to SDS-PAGE (10%) along with normal plasma as the control. For TFRC expression, an equal amount of lysed samples from silenced and wild-type cell lines (HT29, OVCAR3) were resolved on SDS-PAGE (10%) on a Mini-PROTEAN (Biorad, USA) at a constant voltage of 100 V for 2 h. The samples were then transferred to PVDF membranes. The membranes were blocked for 2 h in 5% non-fat dry milk in TBS-Tween at room temperature. Afterwards, blots were incubated with anti-

human transferrin antibody (1:1000, Abcam-ab82411) or anti-transferrin receptor antibody (Invitrogen-136800) overnight incubation at 4 °C. After washing (3x 15 min in TBS-Tween), blots were exposed to a horseradish-conjugated secondary antibody (1:5000, Biorad, USA) for another 1 h at room temperature. The membranes were washed and detected with BM chemiluminescence (Roche, Germany) Western Blotting Substrate. For TFRC, the bands were normalized by a β -actin antibody (1:5000, Santa Cruz-47778). The blots were visualized by Fusion FX Vilber Lourmat (France). Densitometry analysis was performed using Image J software (NIH, Version 1.44).

Determination of Tf

Commercial ELISA kit was employed to measure the Tf content in plasma obtained from patients with various Tf levels. (human transferrin kit by Alpha Diagnostic).

Supplemental References

Supplementary Table 1. Physico-chemical characterization of the bare and functionalized gold nanoparticles (Gold nanorods: Au NRs, Tf: transferrin). The size and zeta potential of the bare and functionalized Au NPs in phosphate buffered saline were determinates by a Malvern Nanosizer.

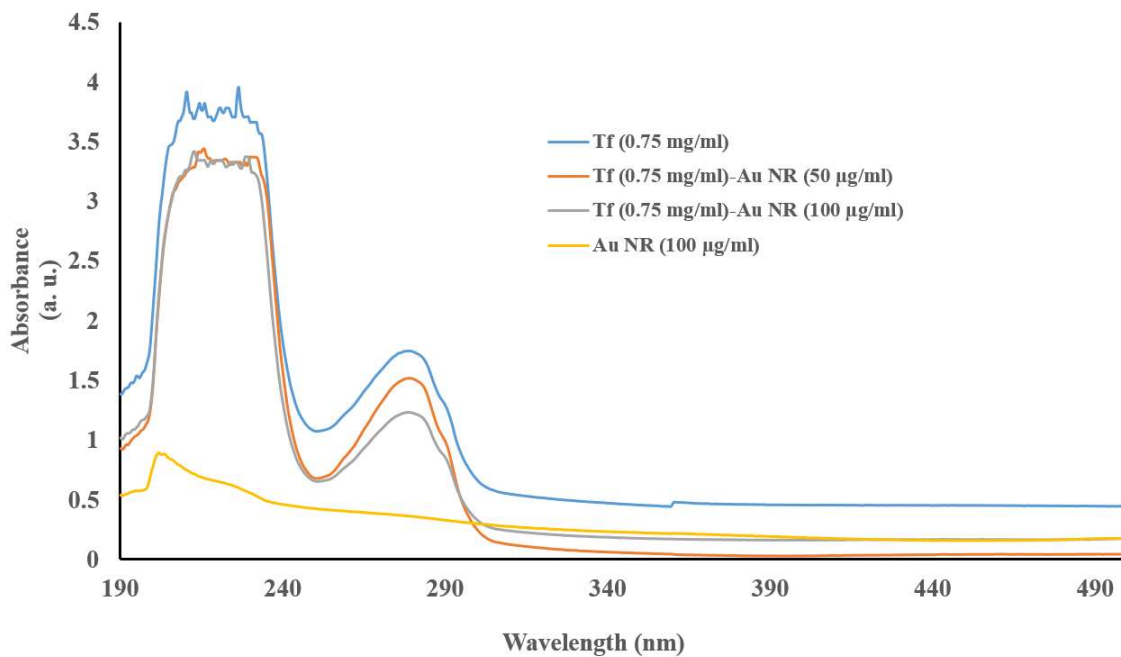
Sample	Average Size (nm)	Zeta potential (mV)	PDI
Seed	12.03±3.96	31.08±5.11	0.233±0.047
Au NRs	43.18±8.27	34.9±7.65	0.407±0.147
Tf-PEG-Au NRs	76.25±6.41	-10.2±2.49	0.603±0.212

Supplementary Table 2. Functionalized gold nanoparticles physicochemical characteristics. (Au NRs: Gold nanorods, Tf: transferrin, HP; Human plasma).

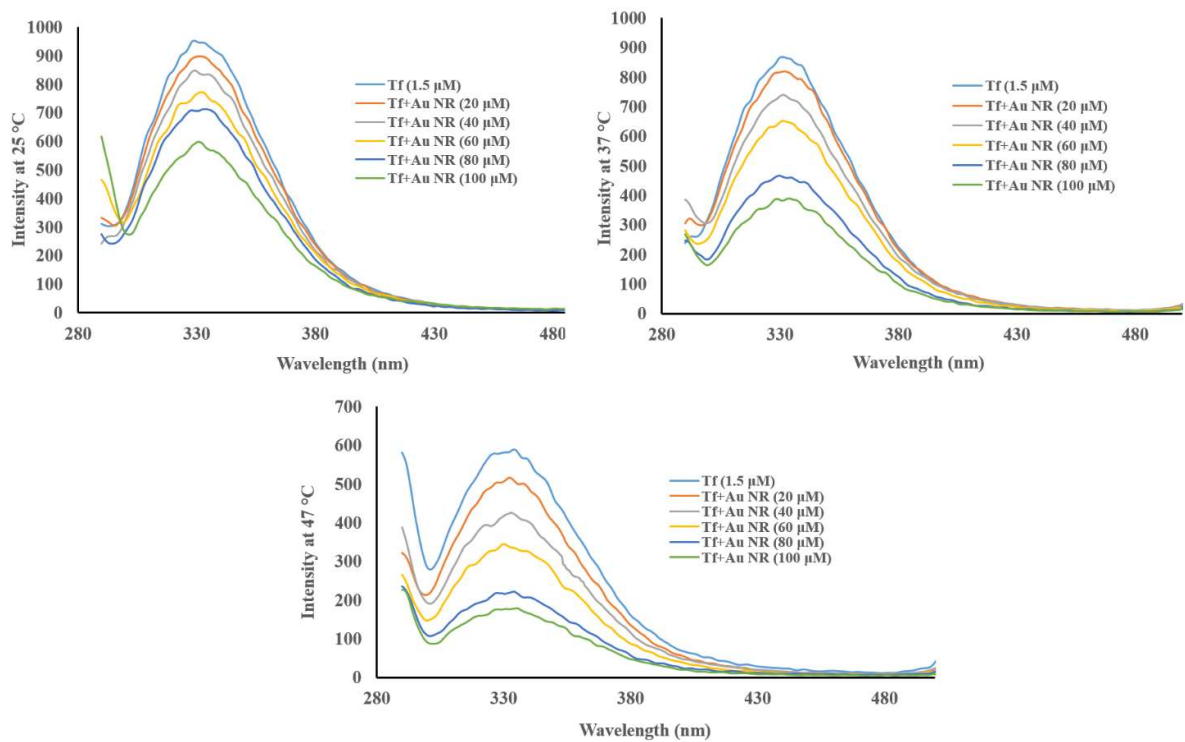
Sample	Type of corona	Average Size (nm)	Zeta potential (mV)	PDI
Tf-PEG-Au NRs	Normal HP 10%	77.32±6.35	-4.54±1.98	0.546
Tf-PEG-Au NRs	Normal HP 50%	88.36±5.34	-5.99±2.28	0.519
Tf-PEG-Au NRs	Tf depleted HP 10%	81.36±4.98	-4.66±3.04	0.577
Tf-PEG-Au NRs	Tf depleted HP 50%	86.54±7.66	-7.45±1.54	0.662
Tf-PEG-Au NRs	Tf excess HP 10%	80.63±6.34	-6.55±2.13	0.509
Tf-PEG-Au NRs	Tf excess HP 50%	91.36±9.65	-8.23±2.71	0.612

Supplementary Table 3. Stern–Volmer constants, binding and thermodynamic parameters of PEGylated Au NRs interaction with Transferrin protein.

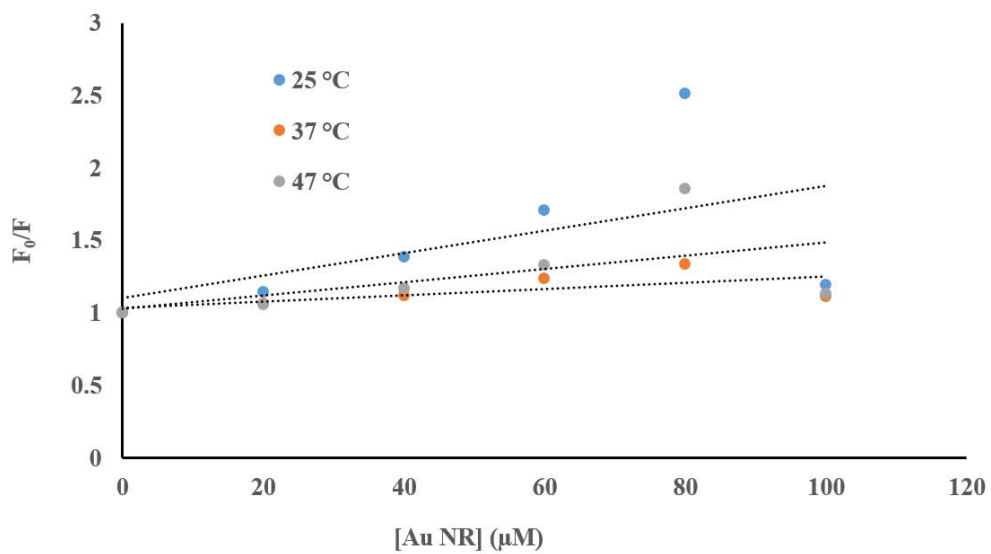
Compound	Temperature (K)	K_{sv} (M^{-1})	K_q ($M^{-1} s^{-1}$)	$K\alpha$ (M^{-1})	n	ΔG ($kJ mol^{-1}$)	ΔH ($kJ mol^{-1}$)	ΔS ($J mol^{-1} K^{-1}$)
	298.15	16952	16952×10^8	3162277.66	1.57	-16.11		
Au NR	310.15	3732.7	3732.7×10^8	151356.12	1.37	-30.73	4012.75	1397.74
	320.15	9134	9134×10^8	50118723.36	1.91	-47.16		



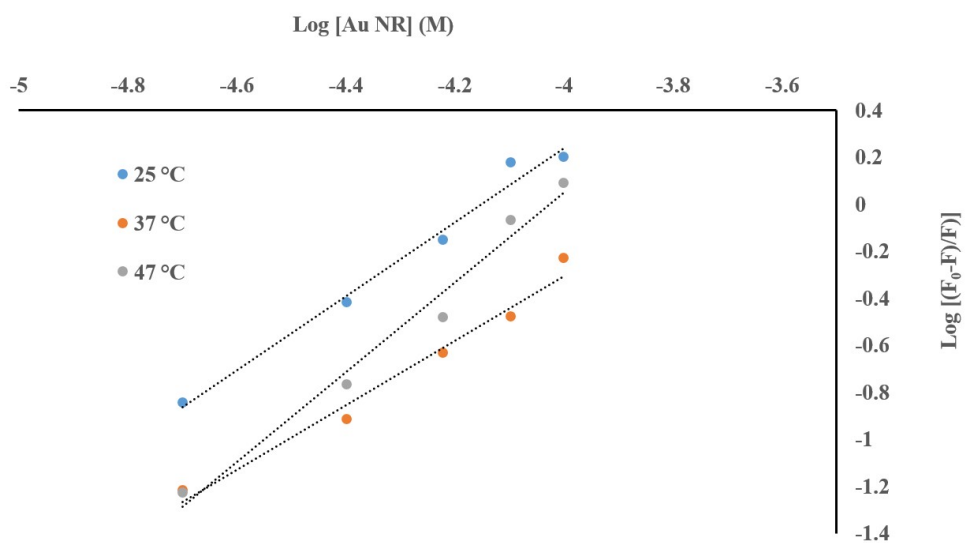
Supplementary Figure 1. The UV-vis absorption spectra of the Tf and PEGylated Gold Nanorods (PEG-Au NRs) complex.



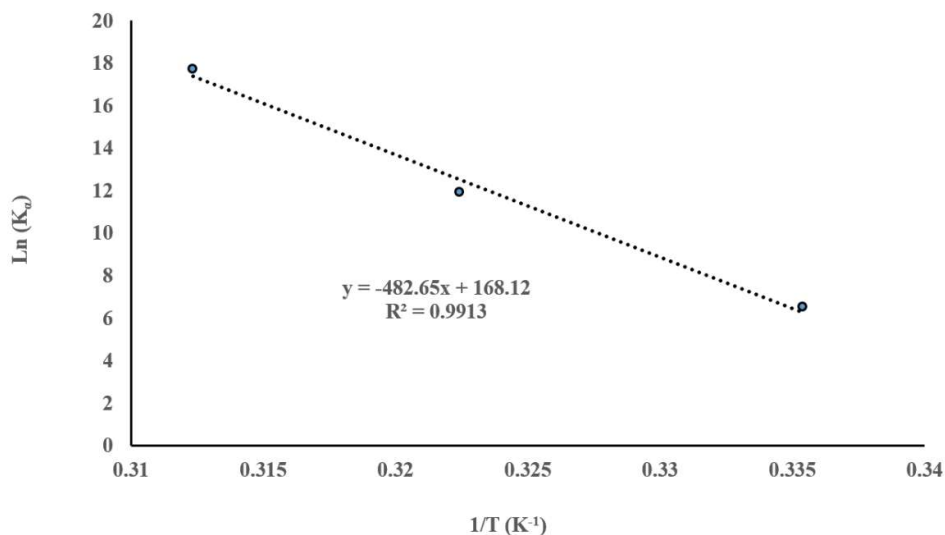
Supplementary Figure 2. Fluorescence intensity of Teransferrin (Tf) protein in the peresence of various concentrations of Gold Nanorods (PEG-Au NRs) in different tempratures (25, 37 and 47 °C).



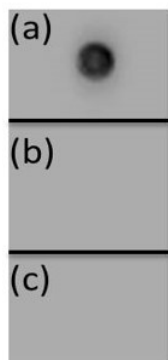
Supplementary Figure 3. The Stern–Volmer plots of Transferrin quenching by different concentrations of PEGylated Au NRs at different temperatures.



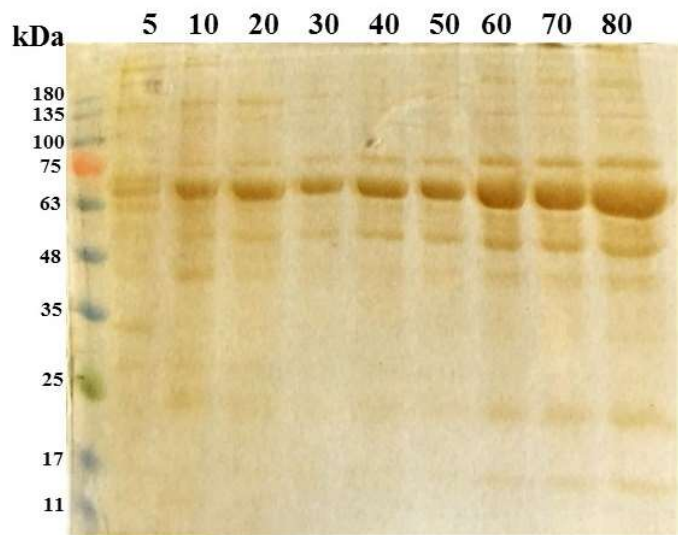
Supplementary Figure 4. The double-log plots Log ((F₀ - F)/F) vs. Log [PEG/Au NRs] for binding of Transferrin with PEGylated Au NRs in different temperatures.



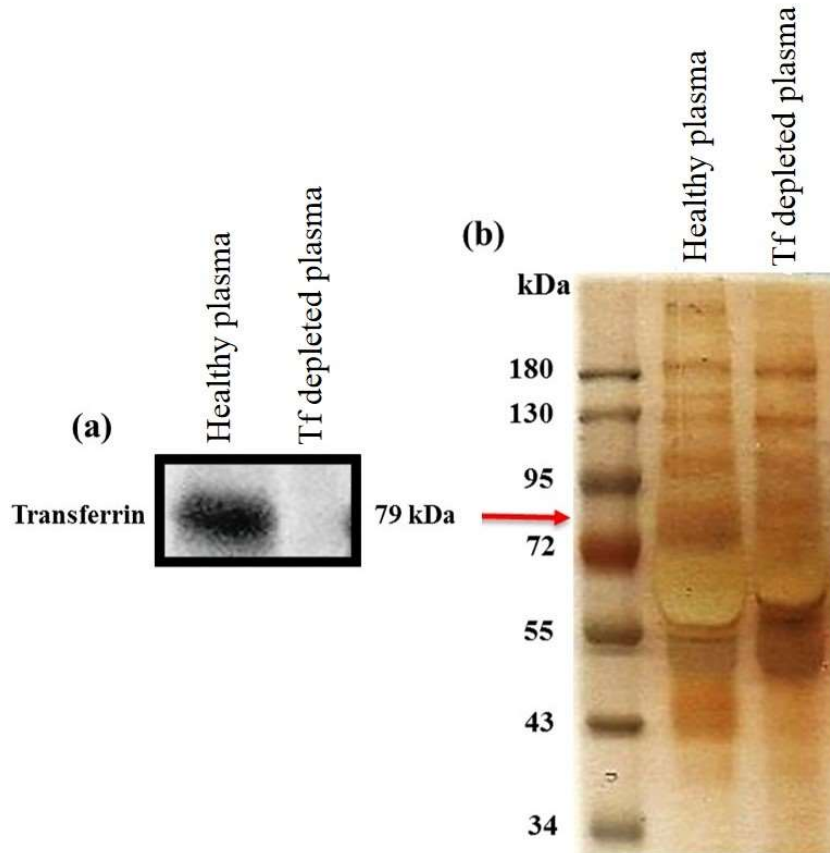
Supplementary Figure 5. The van't Hoff plots of PEG-Au NRs in interaction with Transferrin protein.



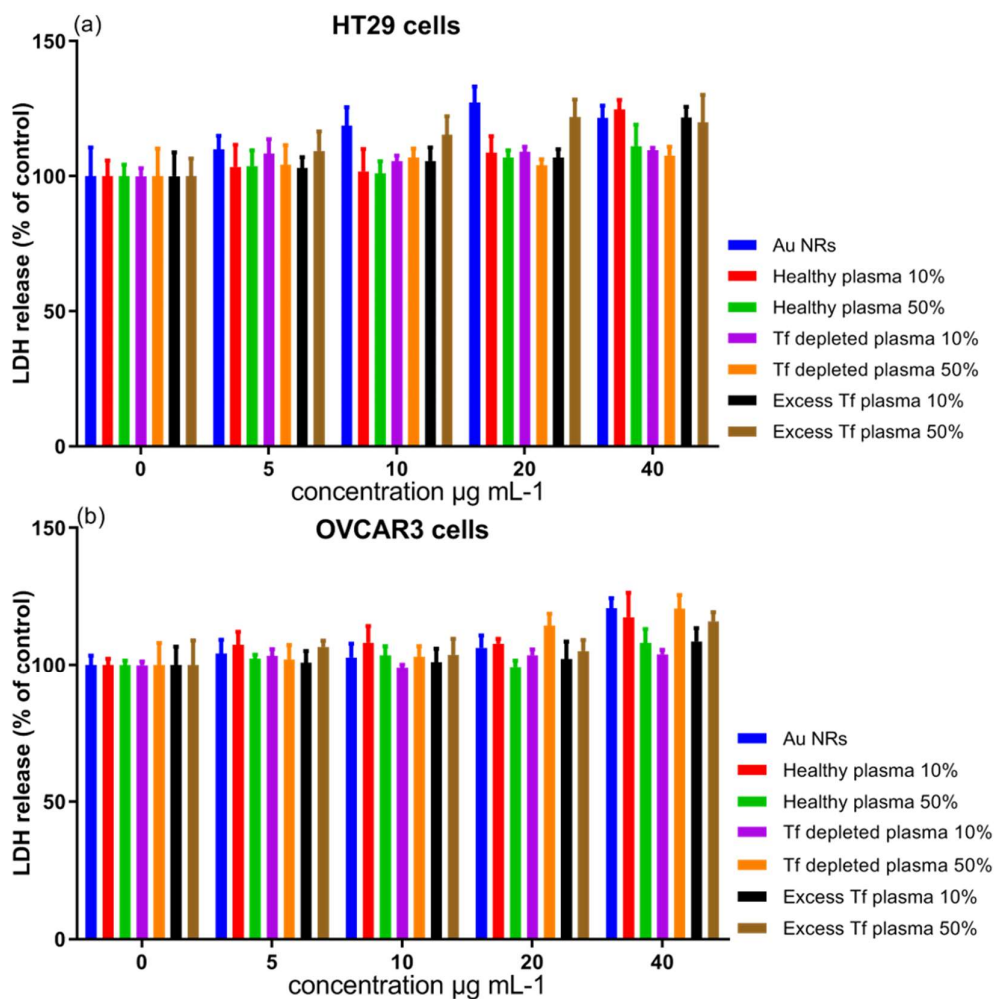
Supplementary Figure 6. Characterization of Tf after binding to gold nanorods (Tf-PEG-Au NRs). Immuno-blot detection of gold nanorods conjugated with human Tf or albumin (Tf-PEG-Au NRs and albumin-PEG-Au NRs, respectively), and the corresponding pegylated precursor (PEG-Au NRs), (a) Tf-PEG-Au NRs, (b) albumin-PEG-Au NRs, and (c) PEG-Au NRs. Primary antibody ($1 \mu\text{L}$ of $100 \mu\text{g mL}^{-1}$) is spotted on the membranes, which were then exposed to the different nanoparticles ($40 \mu\text{g mL}^{-1}$ in PBS). The fluorescence signal of the nanoparticles was detected in the cases where the NPs bound to the antibody on the dot blot. The results indicated that Tf on the Au NRs is recognized by the corresponding antibody, while binding is absent when albumin conjugated with pegylated particles. No unspecific binding was observed for PEG-Au NRs. The data are presented as mean \pm standard error of three independent experiments.



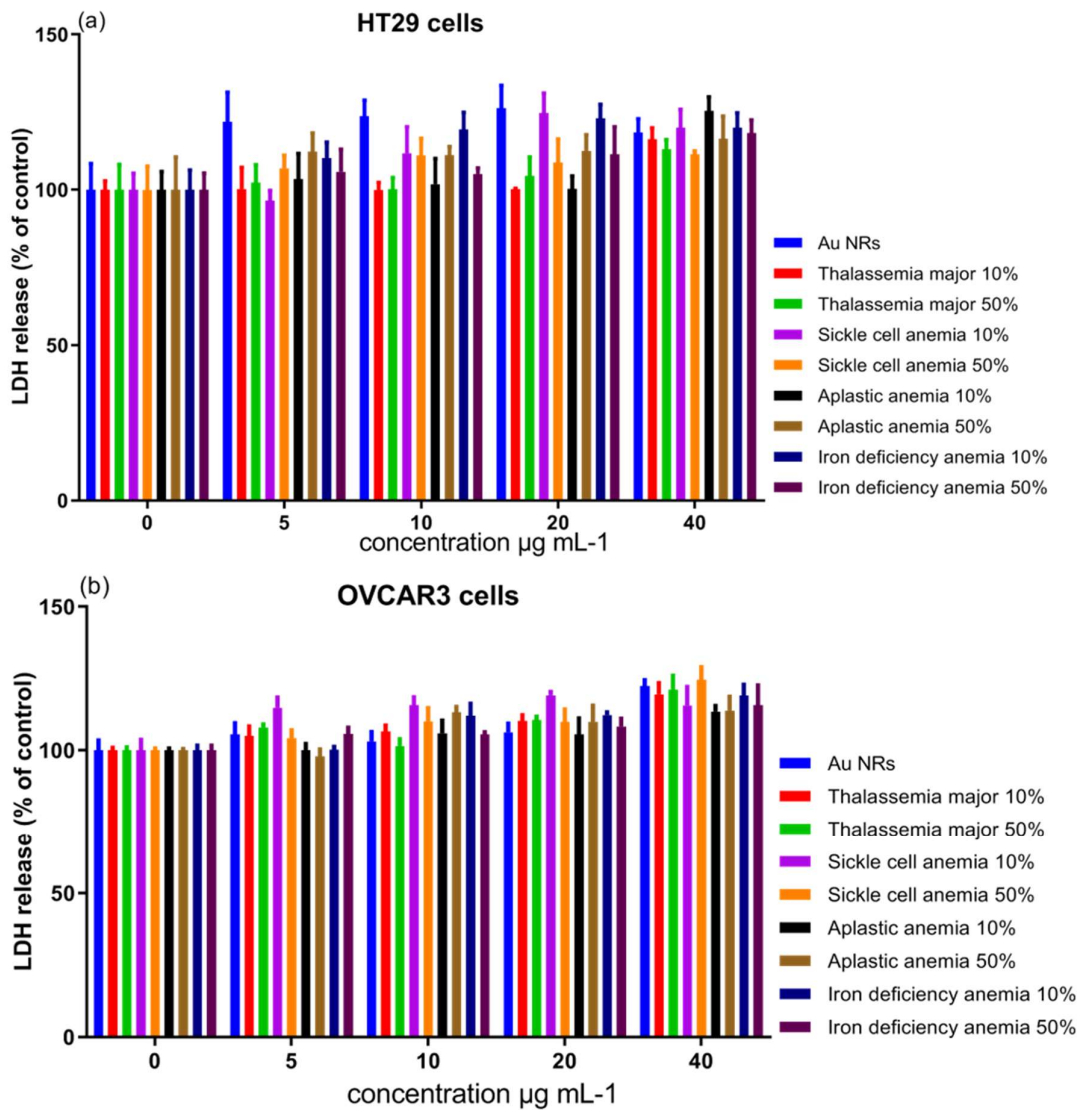
Supplementary Figure 7. SDS-PAGE (10%) of gold nanorods with normal (healthy) human plasma (5-80%)



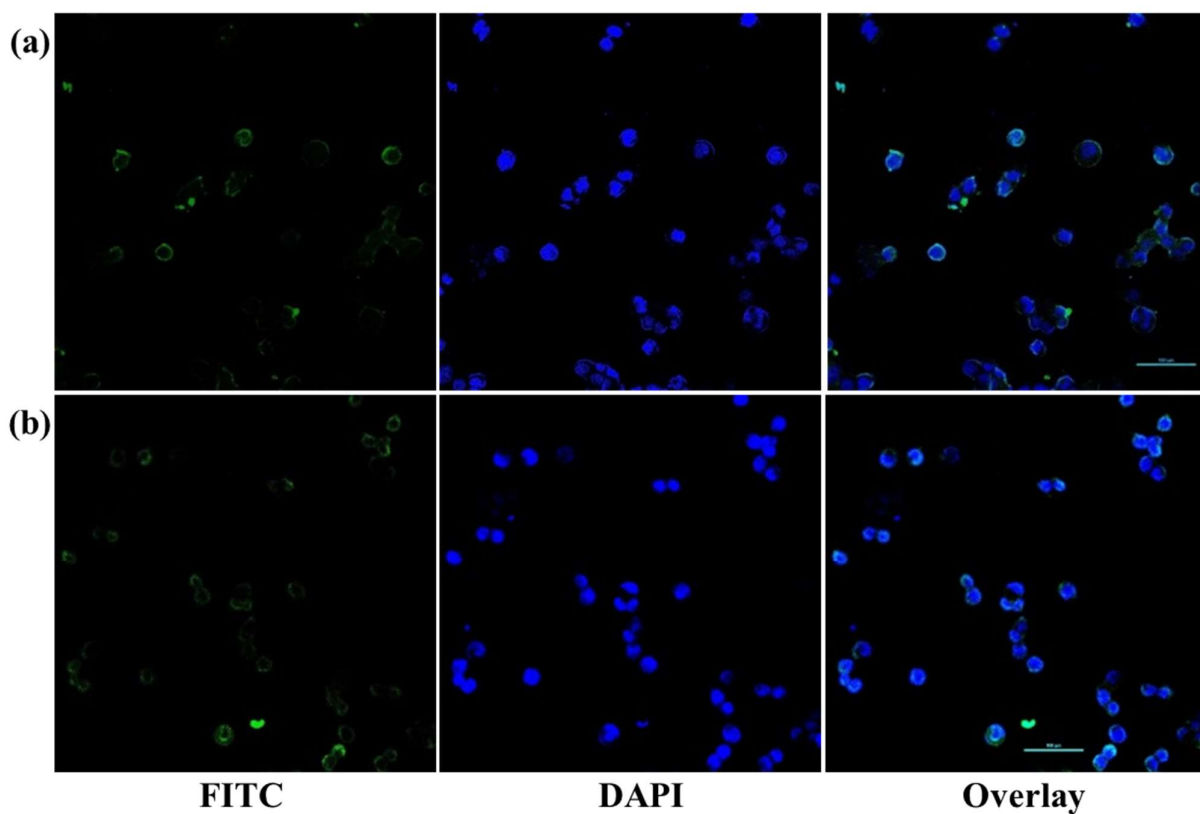
Supplementary Figure 8. Characterization of human serum Tf depletion. (a) Western blot detection of Tf full human plasma proteins and Tf-depleted plasma, and (b) silver nitrate stained SDS-PAGE gel of human serum proteins before and after depletion of endogenous Tf. The protocols of Tf-depletion are described in the Methods part of the main manuscript. Acrylamide gel (10%) has been used to obtain optimal separation of the proteins in the region of interest. Sample loaded from the left are the molecular weight ladder (kDa), full human plasma, and Tf-depleted plasma. The data are presented as mean \pm standard error of three independent experiments.



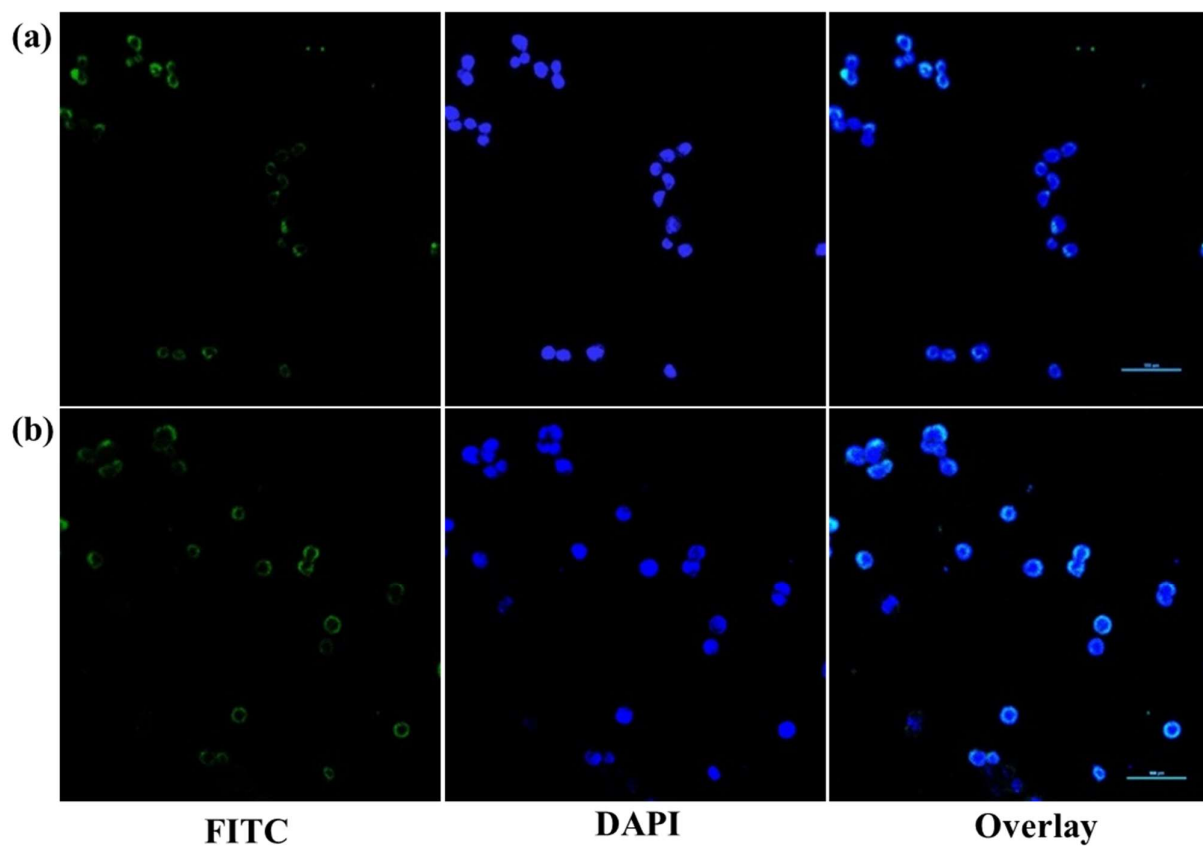
Supplementary Figure 9. The LDH release was measured by the commercial kit as described in materials and methods. (a) HT29 were treated with increasing concentrations of gold nanorods (Au NRs) (from 5 to 40 $\mu\text{g mL}^{-1}$) for 6 h with human plasma (10% and 50%), Tf depleted human serum (10% and 50%) and Tf excess plasma (10% and 50%). (b) OVCAR3 were treated with increasing concentrations of Au NRs (from 5 to 40 $\mu\text{g mL}^{-1}$) for 48 h with healthy human plasma (10% and 50%), Tf depleted human serum (10% and 50%) and Tf excess plasma (10% and 50%). The data are presented as mean \pm standard error of three independent experiments.



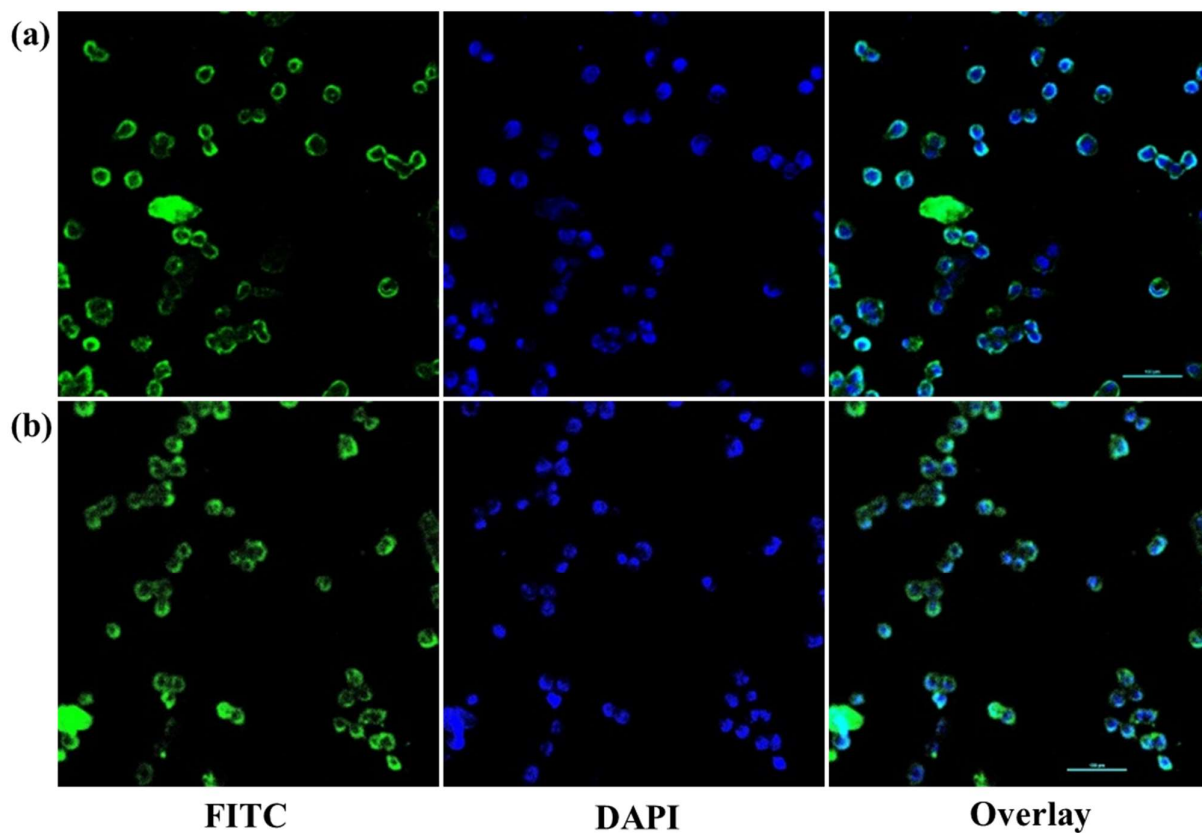
Supplementary Figure 10. The LDH release was determined using the commercial kit. (a) HT29 were treated with increasing concentrations of gold nanorods (Au NRs) (from 5 to 40 $\mu\text{g mL}^{-1}$) for 48 h with thalassemia major, sickle cell anemia, aplastic anemia, and iron deficiency anemia at 10% and 50% plasma concentration. (b) OVCAR3 were treated with increasing concentrations of Au NRs (from 5 to 40 $\mu\text{g mL}^{-1}$) for 48 h with thalassemia major, sickle cell anemia, aplastic anemia, and iron deficiency anemia at 10% and 50% plasma concentration. The data are presented as mean \pm standard error of three independent experiments.



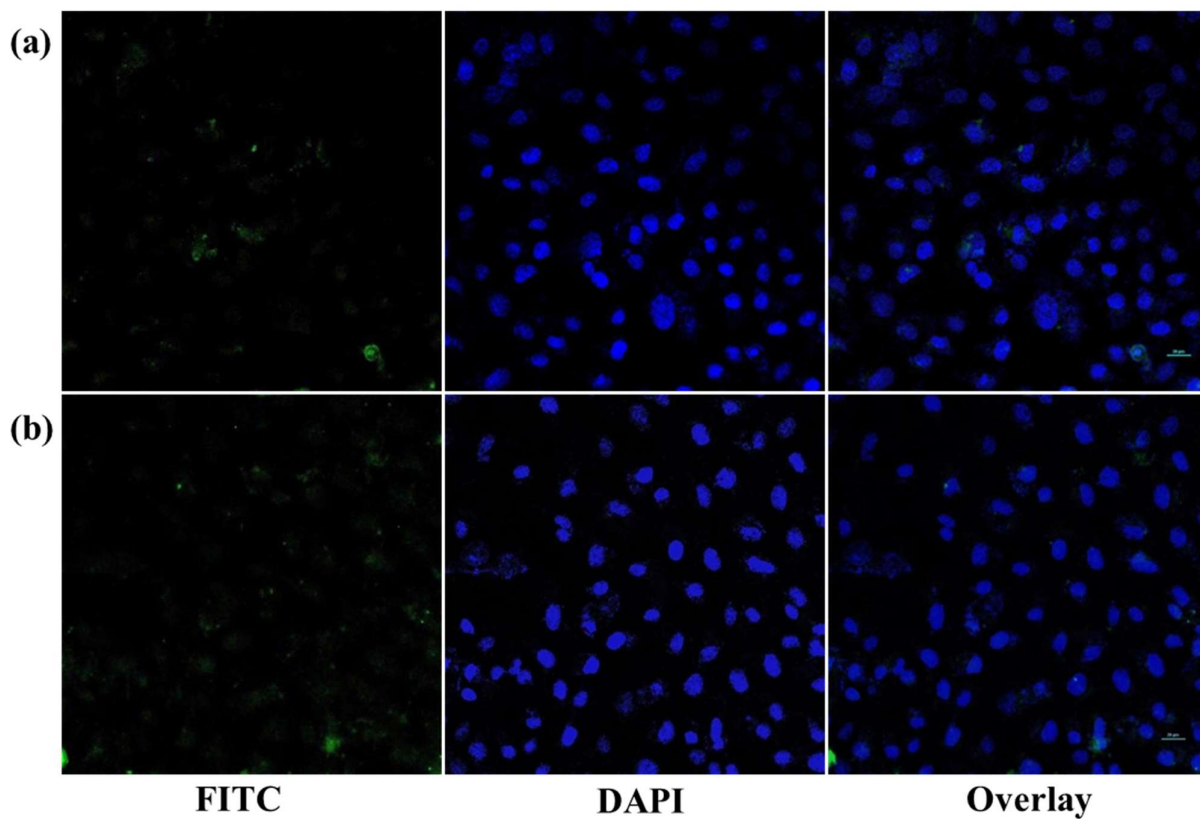
Supplementary Figure 11. Confocal microscopy of the cellular uptake of FITC-labeled gold nanorods in HT29 cells. To clarify endocytosis, uptake studies were done with (a) Gold nanorods coated with healthy plasma (10%), (b) Gold nanorods coated with healthy plasma (50%). Green fluorescence, FITC; blue fluorescence, nuclei stained with DAPI. All pictures are with same magnification and the scale bars represent 20 μm .



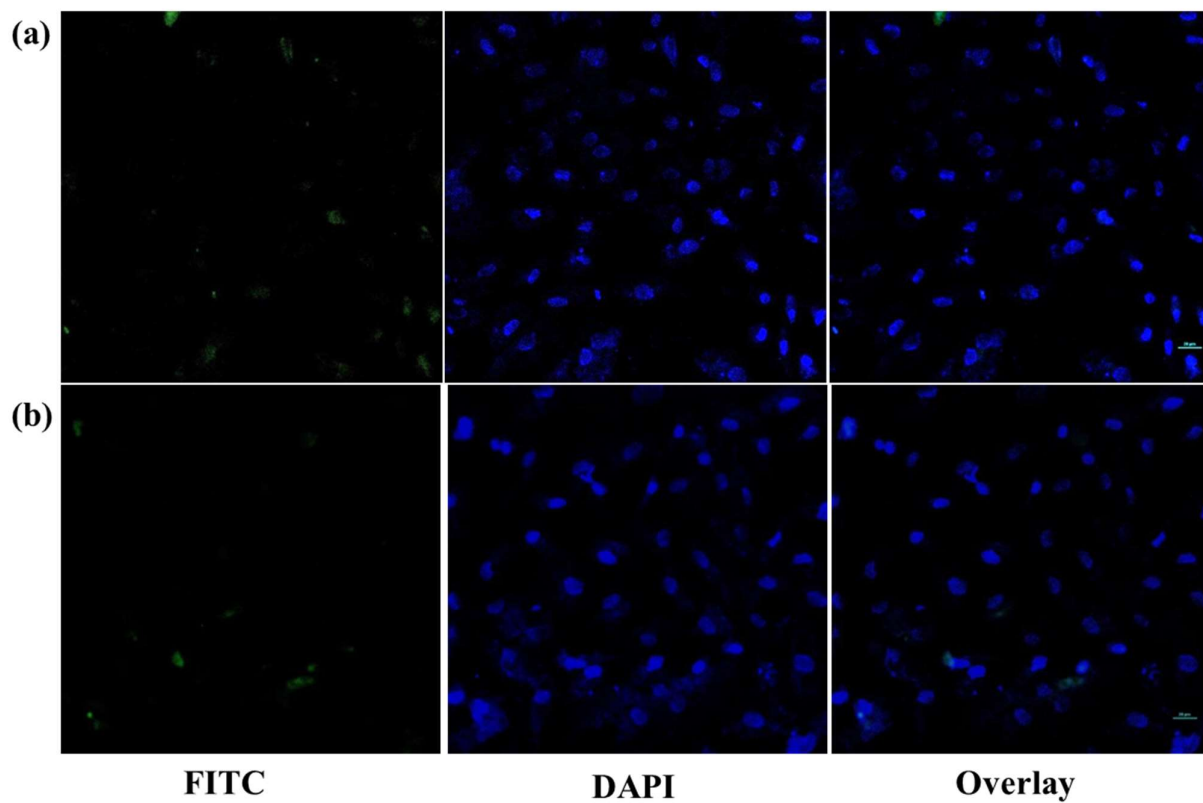
Supplementary Figure 12. Confocal microscopy of the cellular uptake of FITC-labeled gold nanorods in HT29 cells. To clarify endocytosis, uptake studies were done with (a) Gold nanorods coated with transferrin depleted human plasma (10%), (b) Gold nanorods coated with transferrin depleted human plasma (50%). Green fluorescence, FITC; blue fluorescence, nuclei stained with DAPI. All pictures are with same magnification and the scale bars represent 20 μm.



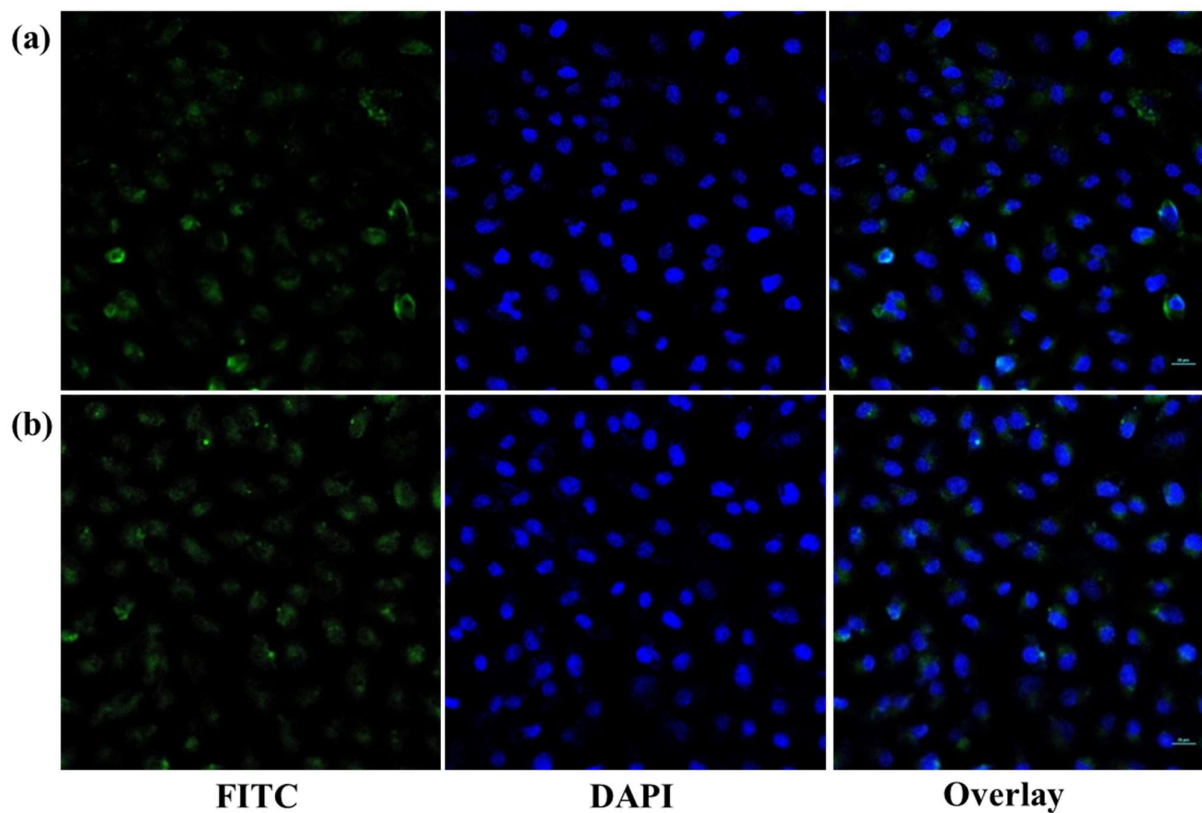
Supplementary Figure 13. Confocal microscopy of the cellular uptake of FITC-labeled gold nanorods in HT29 cells. To clarify endocytosis, uptake studies were done with (a) Gold nanorods coated with Tf excess plasma (10%), (b) Gold nanorods coated with Tf excess plasma (50%). Green florescence, FITC; blue florescence, nuclei stained with DAPI. All pictures are with same magnification and the scale bars represent 20 μm .



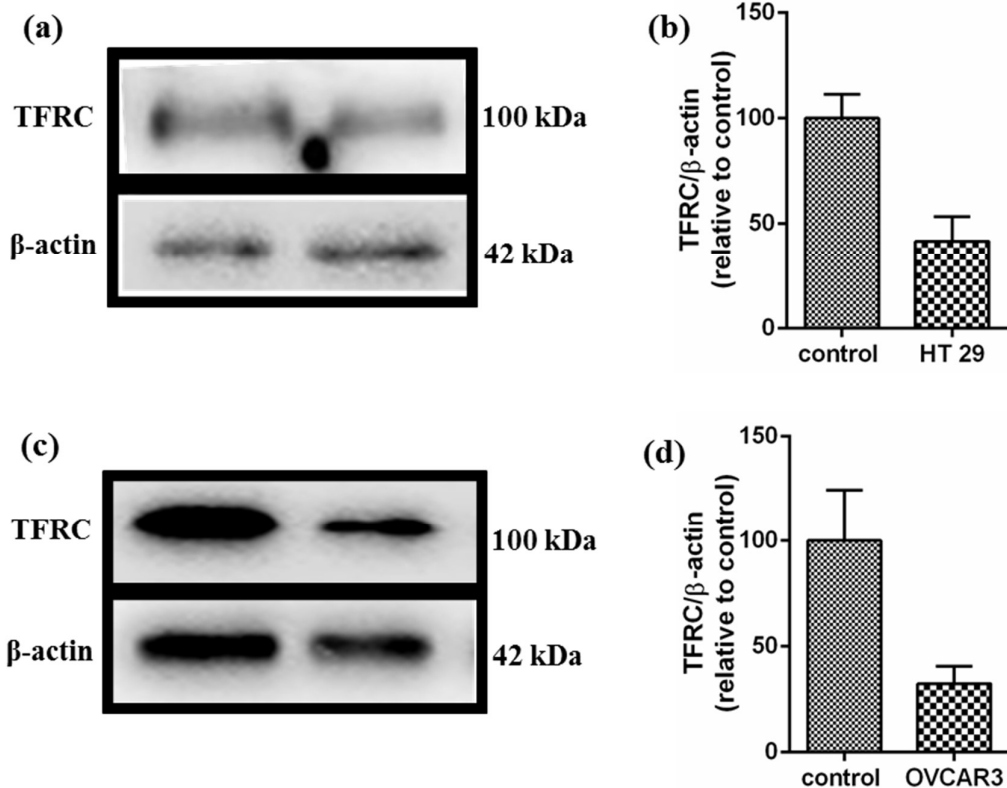
Supplementary Figure 14. Confocal microscopy of the cellular uptake of FITC-labeled gold nanorods in OVCAR3 cells. To clarify endocytosis, uptake studies were done with (a) Gold nanorods coated with healthy plasma (10%), (b) Gold nanorods coated with healthy plasma (50%). Green fluorescence, FITC; blue fluorescence, nuclei stained with DAPI. All pictures are with same magnification and the scale bars represent 20 μm .



Supplementary Figure 15. Confocal microscopy of the cellular uptake of FITC-labeled gold nanorods in OVCAR3 cells. To clarify endocytosis, uptake studies were done with (a) Gold nanorods coated with transferrin depleted human plasma (10%), (b) Gold nanorods coated with transferrin depleted human plasma (50%). Green fluorescence, FITC; blue fluorescence, nuclei stained with DAPI. All pictures are with same magnification and the scale bars represent 20 μm .



Supplementary Figure 16. Confocal microscopy of the cellular uptake of FITC-labeled gold nanorods in OVCAR3 cells. To clarify endocytosis, uptake studies were done with (a) Gold nanorods coated with Tf excess plasma (10%), (b) Gold nanorods coated with Tf excess plasma (50%). Green fluorescence, FITC; blue fluorescence, nuclei stained with DAPI. All pictures are with same magnification and the scale bars represent 20 μm.



Supplementary Figure 17. Western blot analysis of transferrin receptor (TFRC) expressions in HT29 and OVCAR3 cells silenced for the transferrin receptor, (siTFRC). HT29 and OVCAR3 cells are silenced for 72 h as described in the Methods with the transferrin receptor (siTFRC), prior to Western blot assessment. β -actin expression was used as internal control. (a) Western blot analysis indicates that 72 h after treatment, 58.04% of TFRC expression is silenced in HT29 cells. (b) Western blot analysis indicates that 72 h after treatment, 67.58% of TFRC expression is silenced in OVCAR3 cells. The error bars are estimated as mean \pm standard error of three independent experiments.

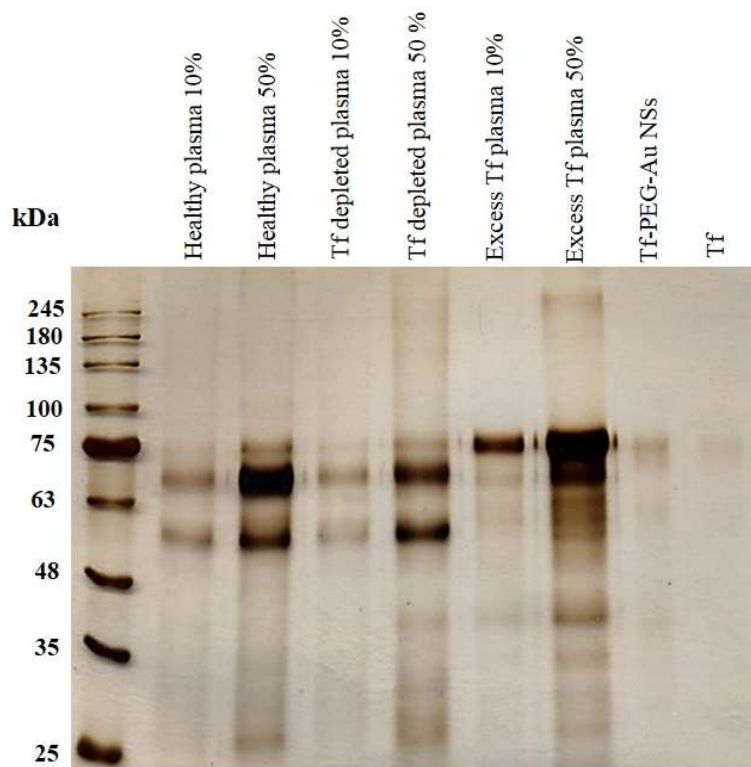
Spherical Gold NPs Data

Supplementary Table 4. Physico-chemical characterization of the bare and functionalized gold nanosphere (Au NSs). The size and zeta potential of the bare and functionalized Au NSs in phosphate buffered saline were determinates by a Malvern Nanosizer. (Tf: transferrin)

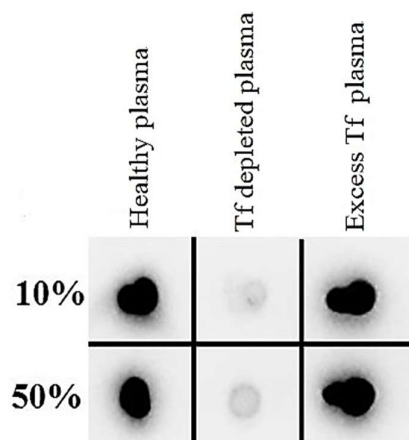
Sample	Average Size (nm)	Zeta potential (mV)	PDI
Tf-PEG-Au NSs	28.7±5.22	-13.8±4.37	0.381±0.144

Supplementary Table 5. Physico-chemical characterization of the bare and functionalized gold nanoparticles (Gold nanosphere: Au NSs, Tf: transferrin). The size and zeta potential of the bare and functionalized Au NSs in phosphate buffered saline were determinates by a Malvern Nanosizer.

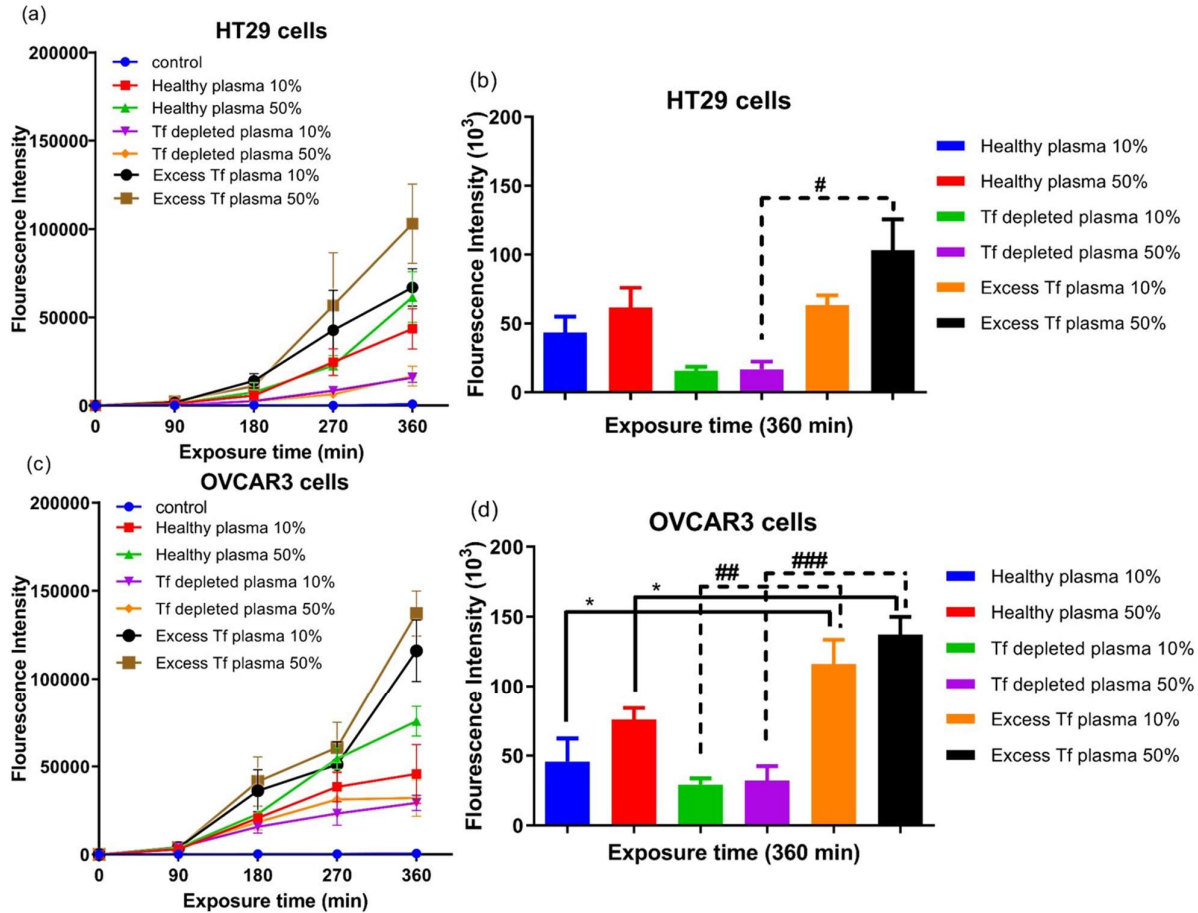
Sample	Type of corona	Average Size (nm)	Zeta potential (mV)	PDI
Tf-PEG-Au NSs	healthy HP 10%	44.21±8.73	-9.12±2.86	0.403
Tf-PEG-Au NSs	healthy HP 50%	48.56±7.66	-11.34±4.91	0.482
Tf-PEG-Au NSs	Tf depleted HP 10%	41.22±11.42	-10.04±3.88	0.422
Tf-PEG-Au NSs	Tf depleted HP 50%	45.44±10.09	-14.21±6.02	0.427
Tf-PEG-Au NSs	Tf excess HP 10%	39.23±7.21	-9.33±3.81	0.511
Tf-PEG-Au NSs	Tf excess HP 50%	44.37±8.33	-10.66±6.28	0.613



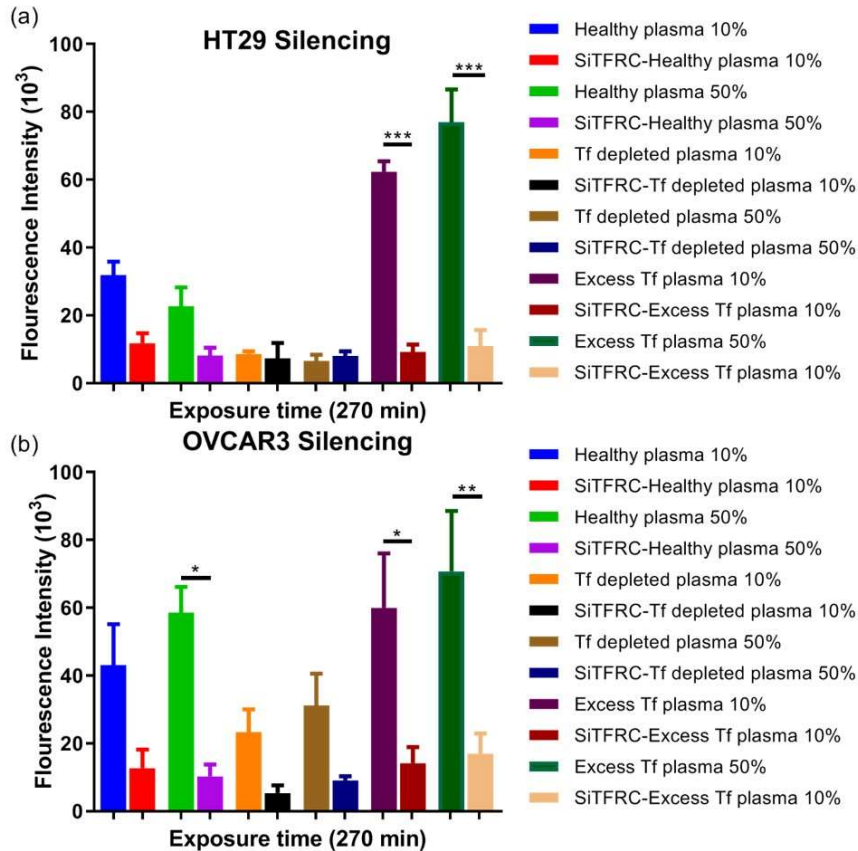
Supplementary Figure 18. SDS-PAGE (10%) of corona coated NPs. Tf-Au NSs after incubation with 10% and 50% of healthy human plasma, Tf depleted human plasma and Tf excess human plasma; Tf-Au NSs and Tf alone were applied as positive control.



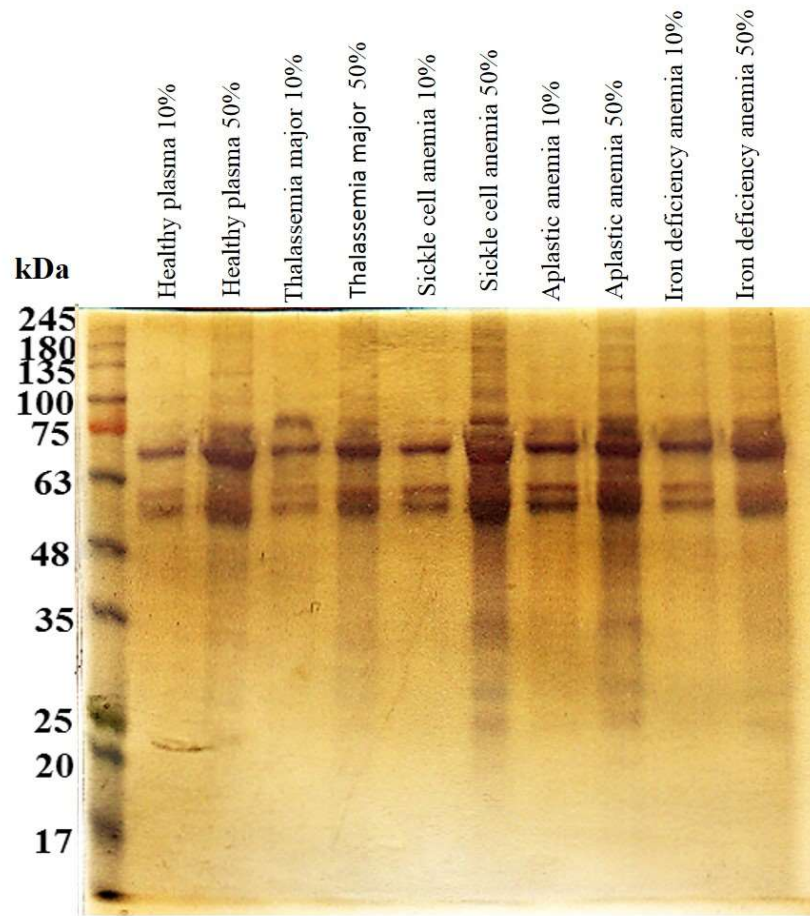
Supplementary Figure 19. Characterization of Tf on Tf–Au NSs coated with protein Immuno-blot detection of Tf on Tf–Au NSs coated with 10% and 50% of healthy human plasma, transferrin depleted human plasma and Tf excess plasma.



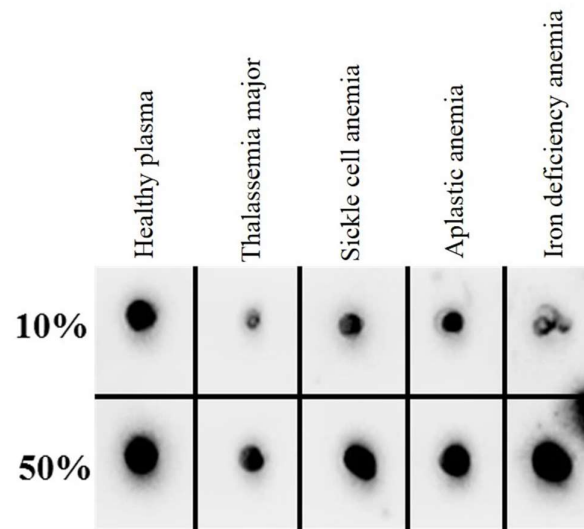
Supplementary Figure 20. Effect of plasma Tf concentration on the uptake of corona-Tf-Au NSs in HT29 and OVCAR3 cells. (a) Median cell fluorescence intensity (MFI) performed by flow cytometry for HT29 cells treated with $40 \mu\text{g mL}^{-1}$ Tf-NPs subjected to healthy human plasma (10% and 50%), Tf depleted human plasma (10% and 50%) and Tf excess plasma (10% and 50%) in serum free RPMI. (b) MFI performed by flow cytometry for HT29 cells treated with corona-Tf-Au NSs at 360 min exposure in serum free medium. (c) MFI performed by flow cytometry for OVCAR3 cells treated with $40 \mu\text{g mL}^{-1}$ corona-Tf-Au NSs subjected to healthy human plasma (10% and 50%), Tf depleted human plasma (10% and 50%) and Tf excess plasma (10% and 50%) in serum free DMEM. (d) MFI performed by flow cytometry for OVCAR3 cells treated with $40 \mu\text{g mL}^{-1}$ corona-Tf-Au NSs at 360 min exposure in serum free medium. The error bars are estimated as mean \pm standard error of three independent samples and at least 10 000 cells were analyzed in each experiment. * $p < 0.05$, # $p < 0.05$, and ### $p < 0.01$.



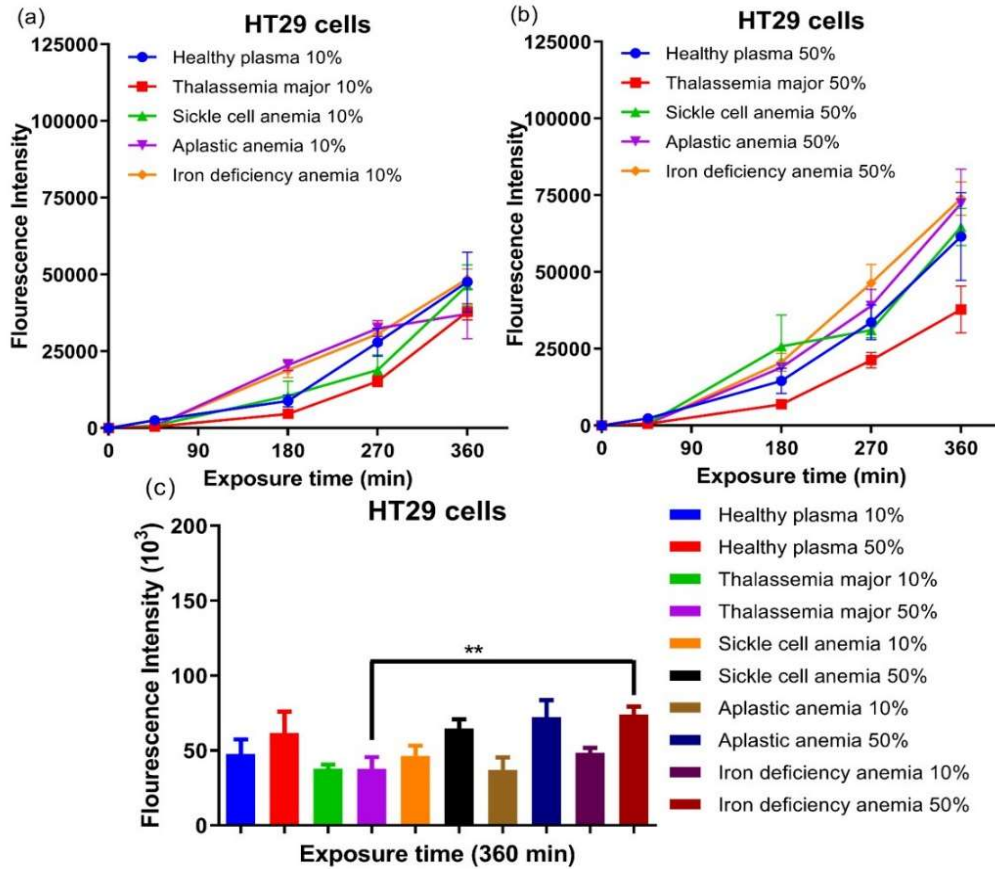
Supplementary Figure 21. MFI performed by flow cytometry for HT29 and OVCAR3 treated with $40 \mu\text{g ml}^{-1}$ corona-Tf-Au NSs subjected to healthy human plasma (10 % and 50%), Tf depleted human plasma (10% and 50%) and Tf excess plasma (10% and 50%) in serum free medium, presenting that the uptake is drastically reduced in TFRC silenced cells. HT29 and OVCAR3 cells are silenced for 72 h (as defined in the Methods) with SiTFRC before exposure to NPs ($40 \mu\text{g mL}^{-1}$, for 270 min) in serum-free medium. However, other (non-TFRC) pathways still contribute to cellular uptake of some NPs. The error bars are estimated as mean \pm standard error of three independent samples and at least 10 000 cells were analyzed in each experiment. * $p < 0.05$, ** $p < 0.01$, and *** $p < 0.001$.



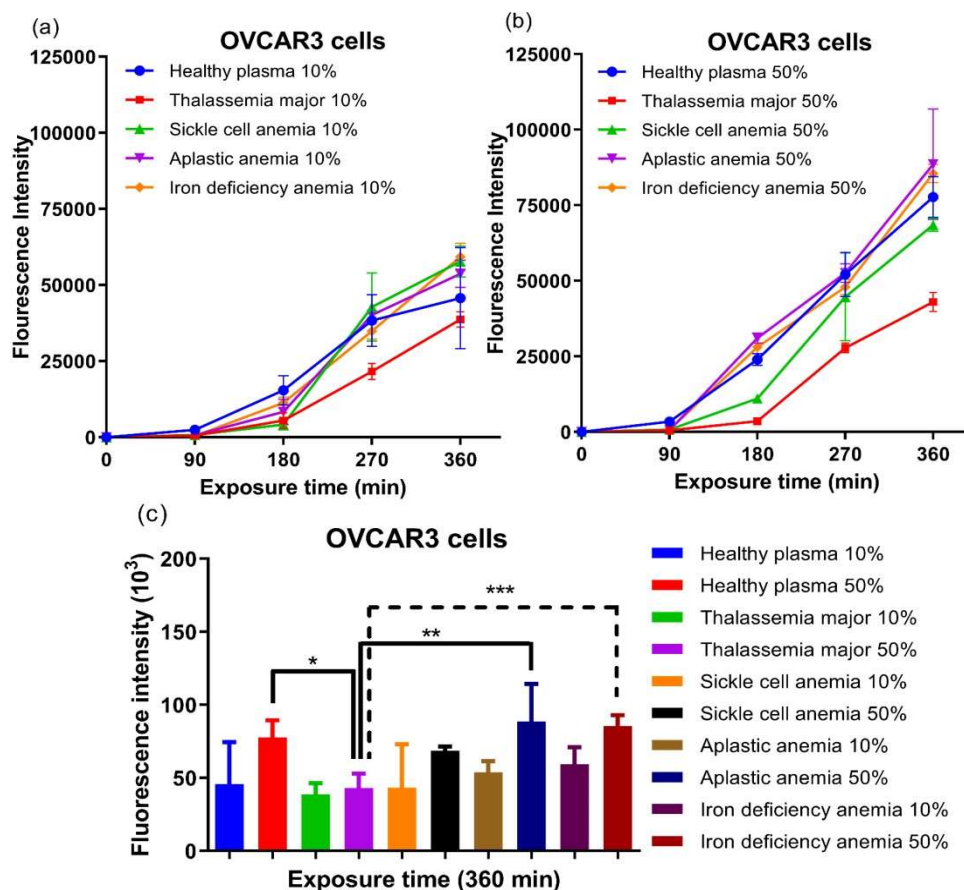
Supplementary Figure 22. SDS-PAGE (10%) of Tf-PEG-Au NSs coated with plasma that were obtained from volunteers with different types of diseases/conditions, including healthy, thalassemia major, sickle cell anemia, aplastic anemia, and iron deficiency anemia.



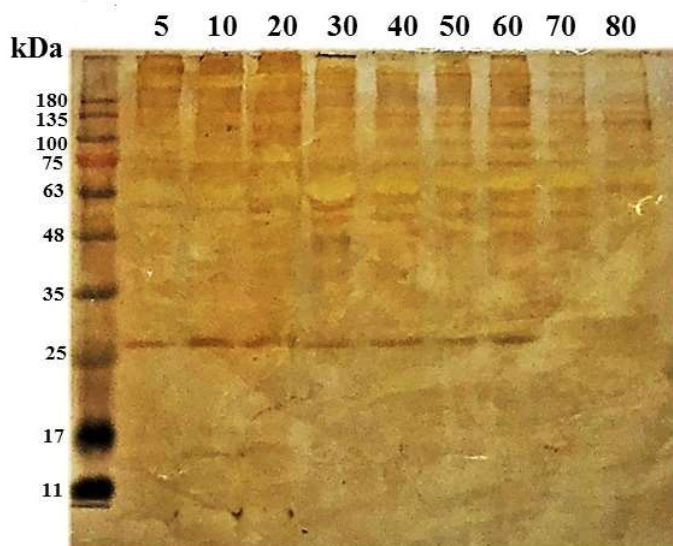
Supplementary Figure 23. Characterization of Tf on gold nanospheres (Au NSs) surface coated with protein corona. Immuno-blot detection of Tf on Tf-PEG-Au NSs coated with plasmas that were obtained from volunteers with different types of diseases/conditions, including healthy, thalassemia major, Sickle cell anemia, Aplastic anemia, and Iron deficiency anemia.



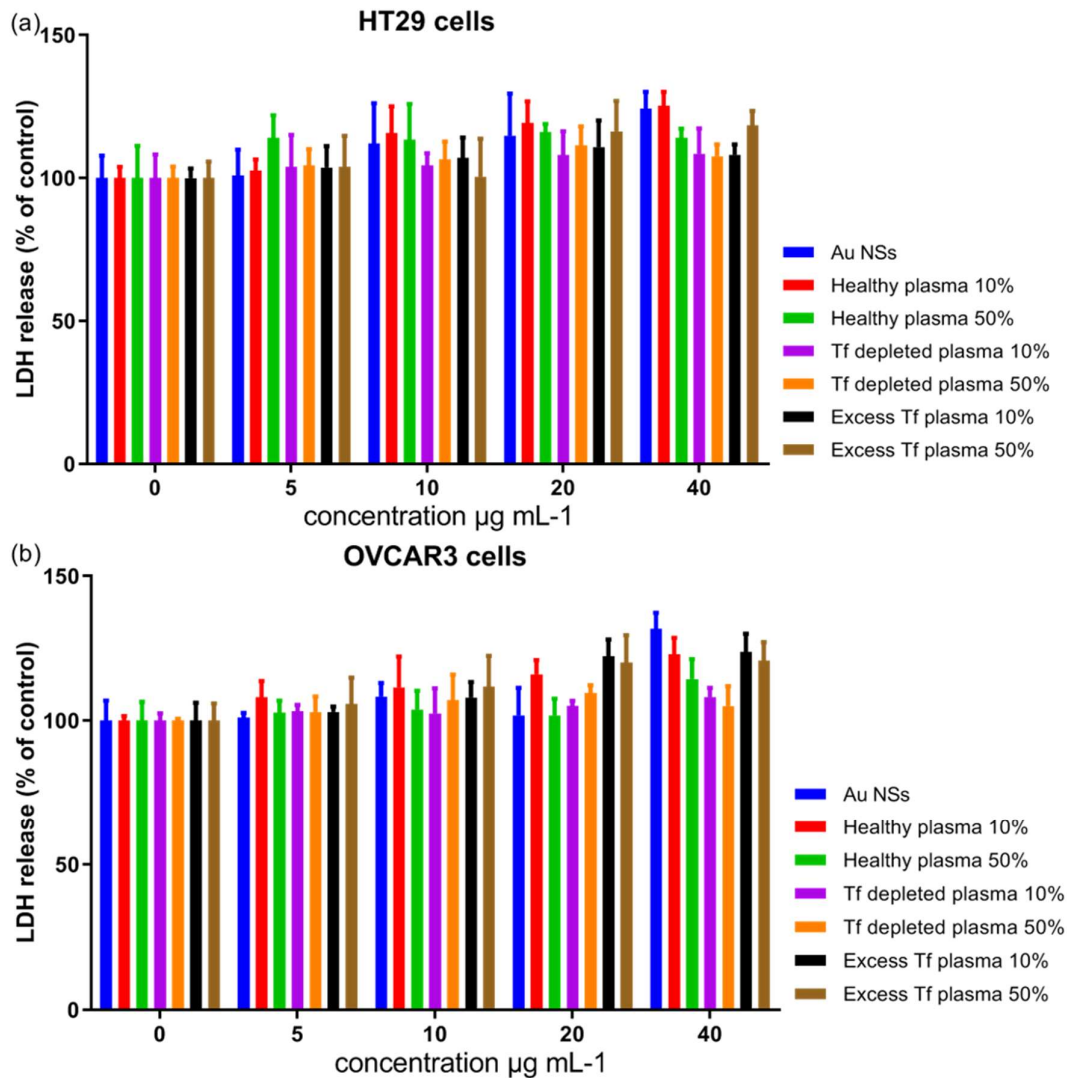
Supplementary Figure 24. Effect of Tf concentration on the uptake of the corresponding corona-Tf-Au NSs in HT29 cells. MFI performed by flow cytometry for HT29 cells treated with $40 \mu\text{g mL}^{-1}$ corona-Tf-Au NSs subjected to healthy, thalassemia major, sickle cell anemia, aplastic anemia, and iron deficiency anemia (a) at 10% plasma concentration and (b) at 50% plasma concentration (c) at 360 min exposure in serum free RPMI. The error bars are estimated as mean \pm standard error of three independent samples and at least 10 000 cells were analyzed in each experiment.



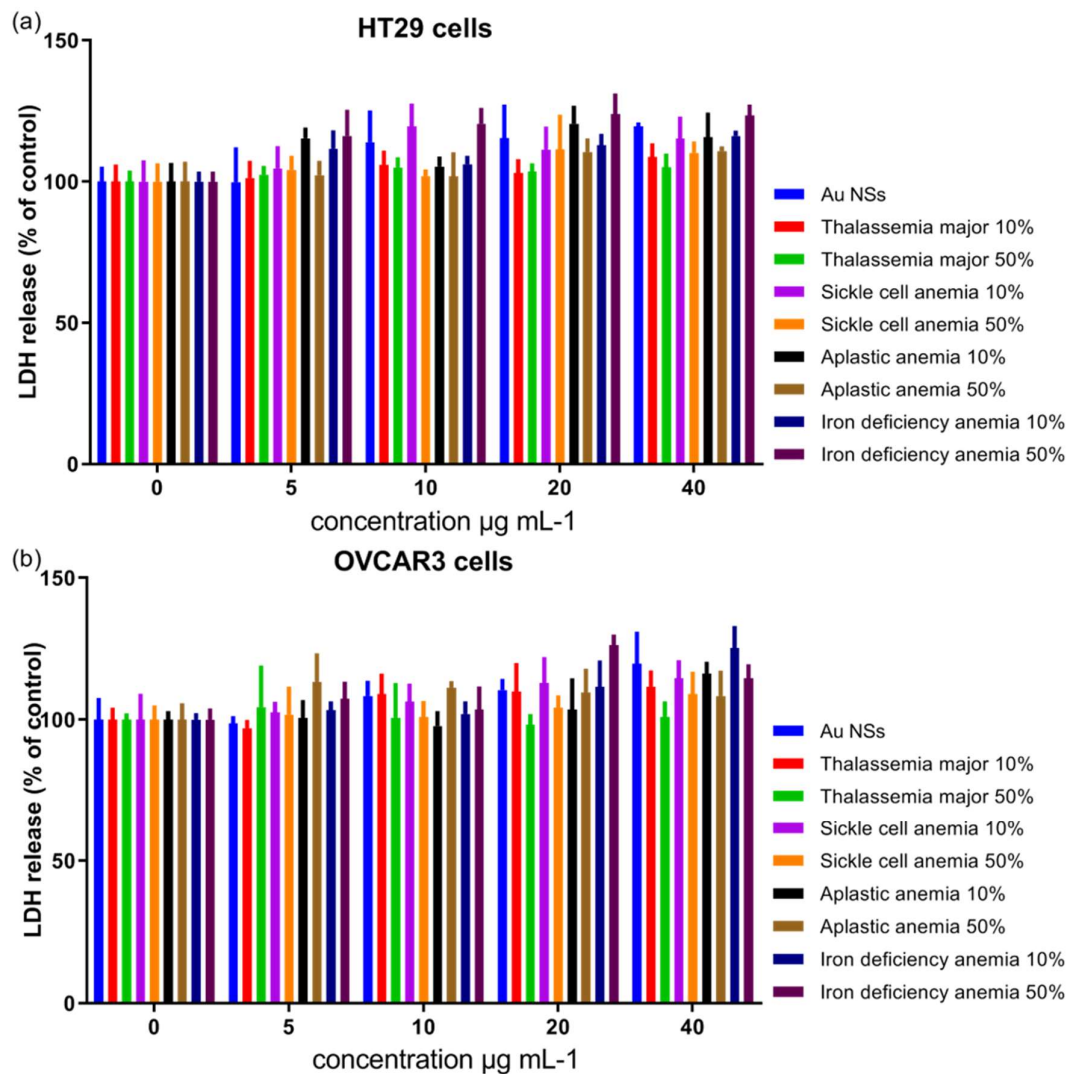
Supplementary Figure 25. Effect of Tf concentration on the uptake of the corresponding corona-Tf-Au NSs in OVCAR3 cells. MFI performed by flow cytometry for OVCAR3 cells exposed with $40 \mu\text{g mL}^{-1}$ corona-Tf-Au NSs subjected to healthy, thalassemia major, sickle cell anemia, aplastic anemia, and iron deficiency anemia (a) at 10% plasma concentration and (b) at 50% plasma concentration (c) at 360 min exposure in serum free DMEM. The error bars are estimated as mean \pm standard error of three independent samples and at least 10 000 cells were analyzed in each experiment. * $p < 0.05$, ** $p < 0.01$.



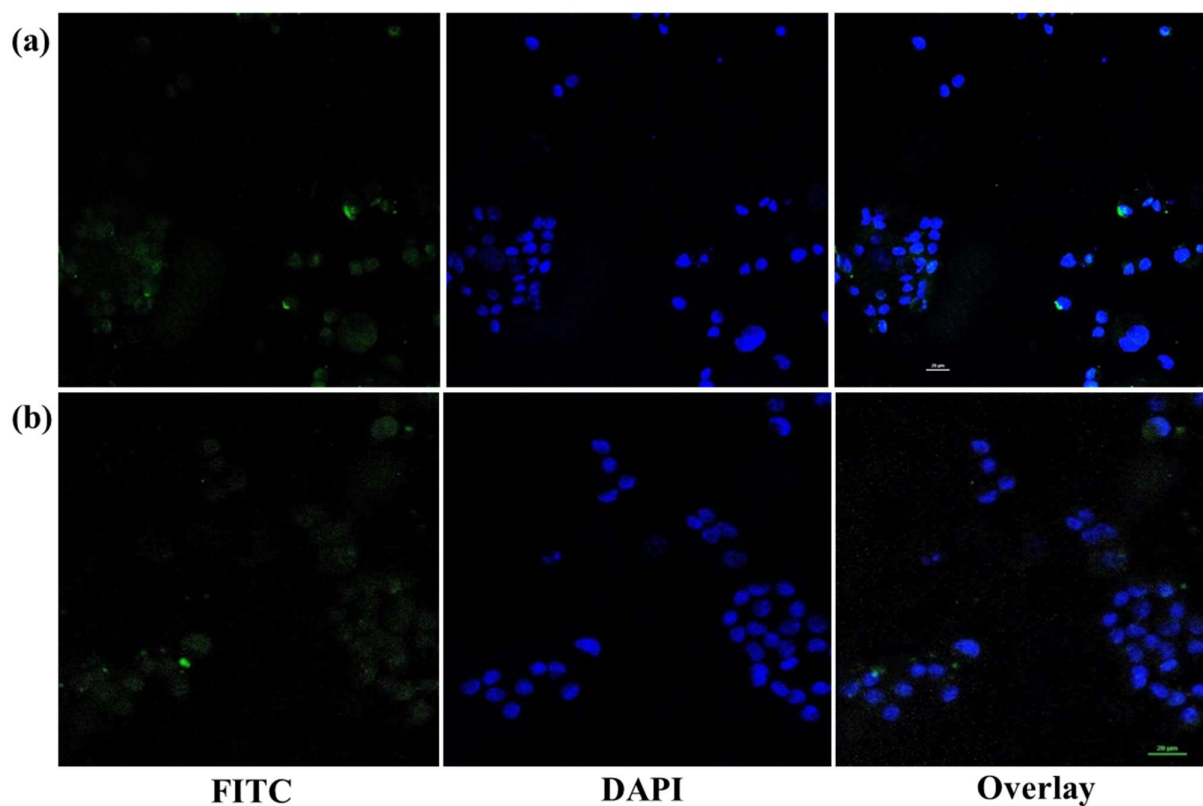
Supplementary Figure 26. SDS-PAGE (10%) of (a) gold nanospheres (Au NSs) with healthy human plasma (5-80%).



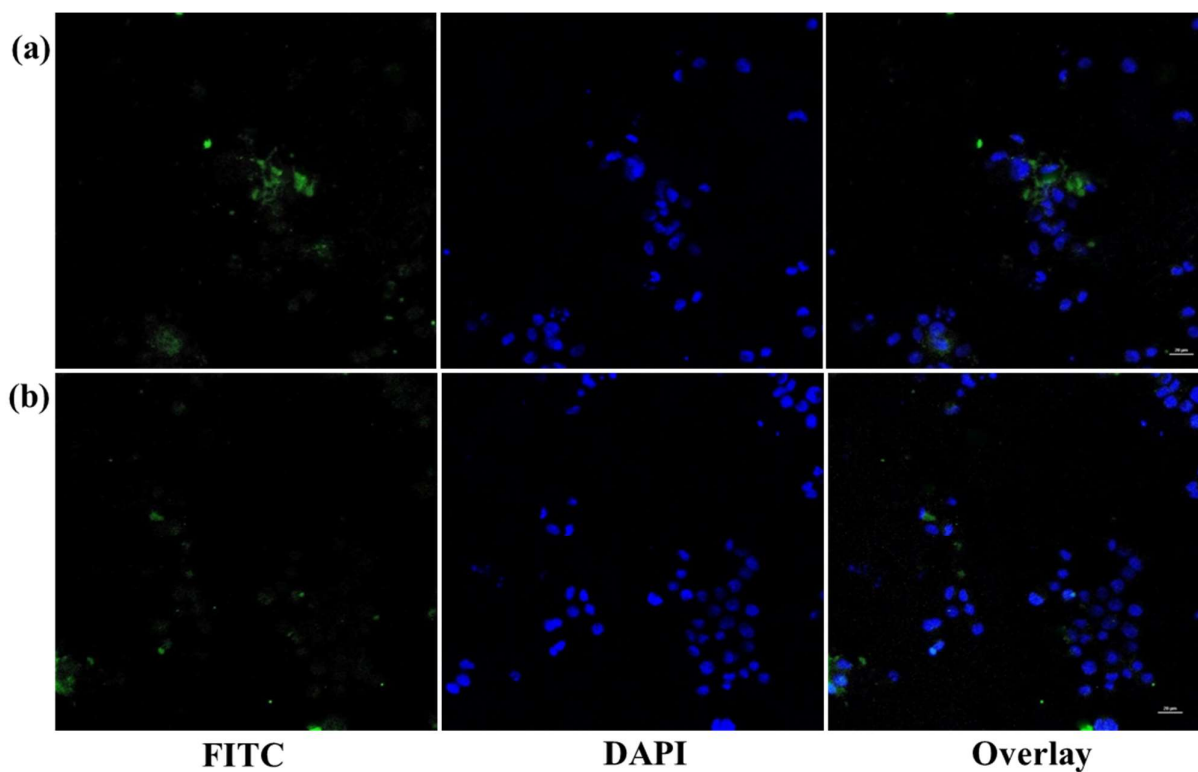
Supplementary Figure 27. The LDH release was measured by the commercial kit as described in materials and methods. (a) HT29 were treated with increasing concentrations of gold nanospheres (Au NSs) (from 5 to 40 $\mu\text{g mL}^{-1}$) for 6 h with human plasma (10% and 50%), Tf depleted human serum (10% and 50%) and Tf excess plasma (10 and 50%). (b) OVCAR3 were treated with increasing concentrations of Au NSs (from 5 to 40 $\mu\text{g mL}^{-1}$) for 48 h with healthy human plasma (10 and 50%), Tf depleted human serum (10 and 50%) and Tf excess plasma (10% and 50%). The data are presented as mean \pm standard error of three independent experiments.



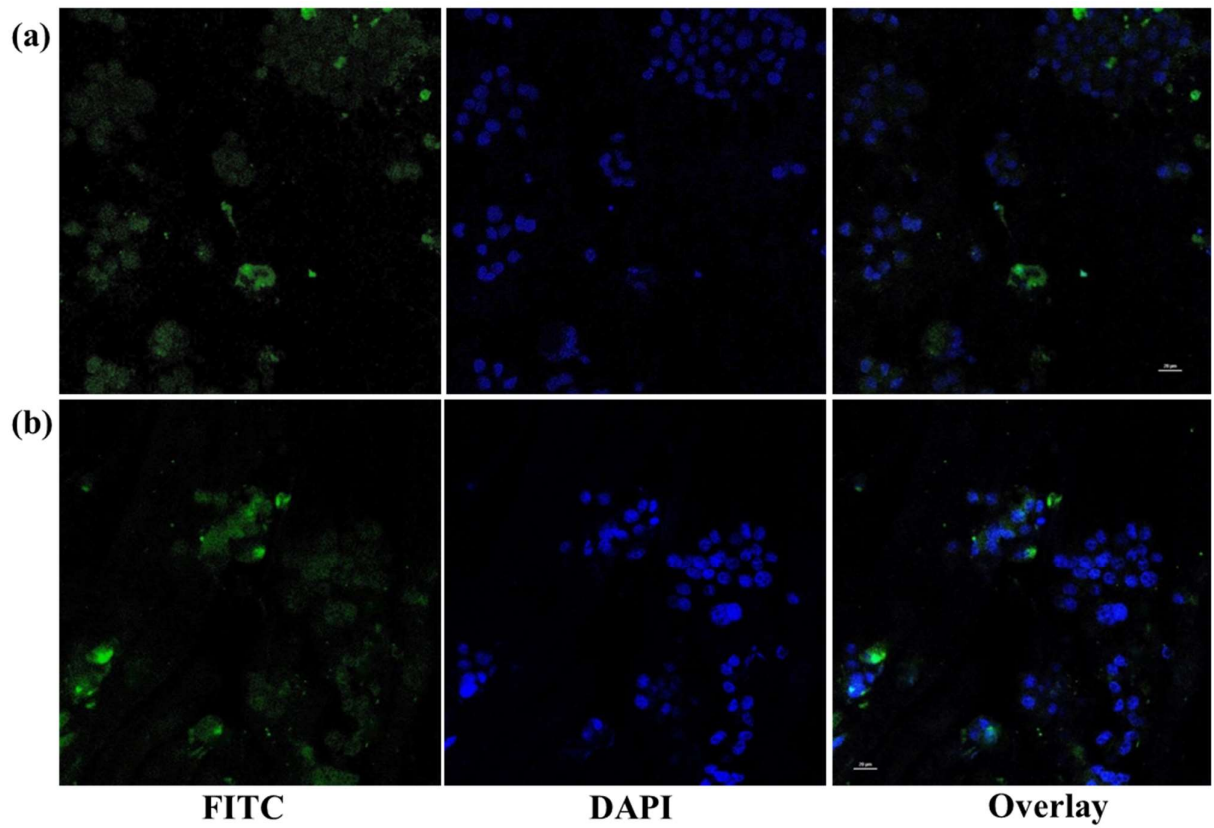
Supplementary Figure 28. The LDH release was determined using the commercial kit. (a) HT29 were treated with increasing concentrations of gold nanospheres (Au NSs) (from 5 to 40 $\mu\text{g mL}^{-1}$) for 48 h with thalassemia major, sickle cell anemia, aplastic anemia, and iron deficiency anemia at 10% and 50% plasma concentration. (b) OVCAR3 were treated with increasing concentrations of (a) Au NSs (from 5 to 40 $\mu\text{g mL}^{-1}$) for 48 h with thalassemia major, sickle cell anemia, aplastic anemia, and iron deficiency anemia at 10% and 50% plasma concentration. The data are presented as mean \pm standard error of three independent experiments.



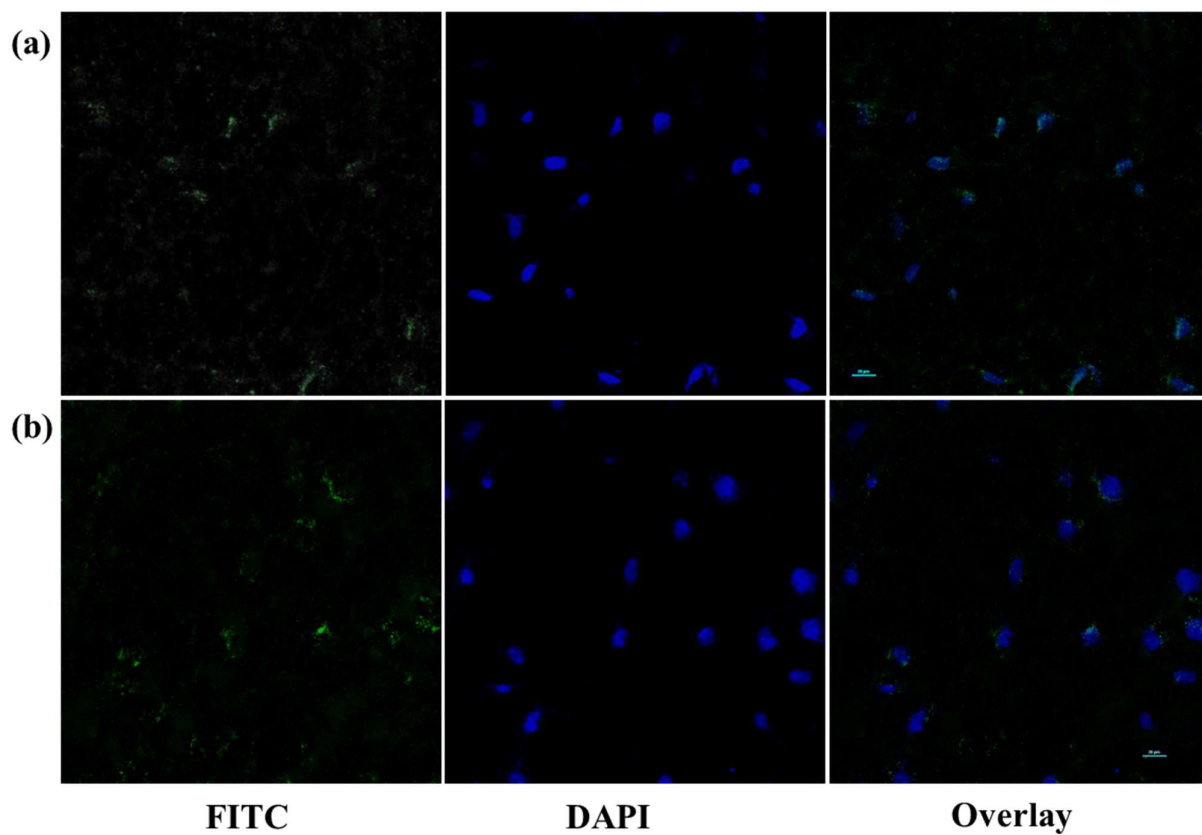
Supplementary Figure 29. Confocal microscopy of the cellular uptake of FITC-labeled Tf-conjugated gold nanospheres in HT29 cells. To clarify endocytosis, uptake studies were done with (a) healthy human plasma coated gold nanospheres (10%), (b) healthy human plasma coated gold nanospheres (50%). Green fluorescence, FITC; blue fluorescence, nuclei stained with DAPI. All pictures are with same magnification and the scale bars represent 20 μm .



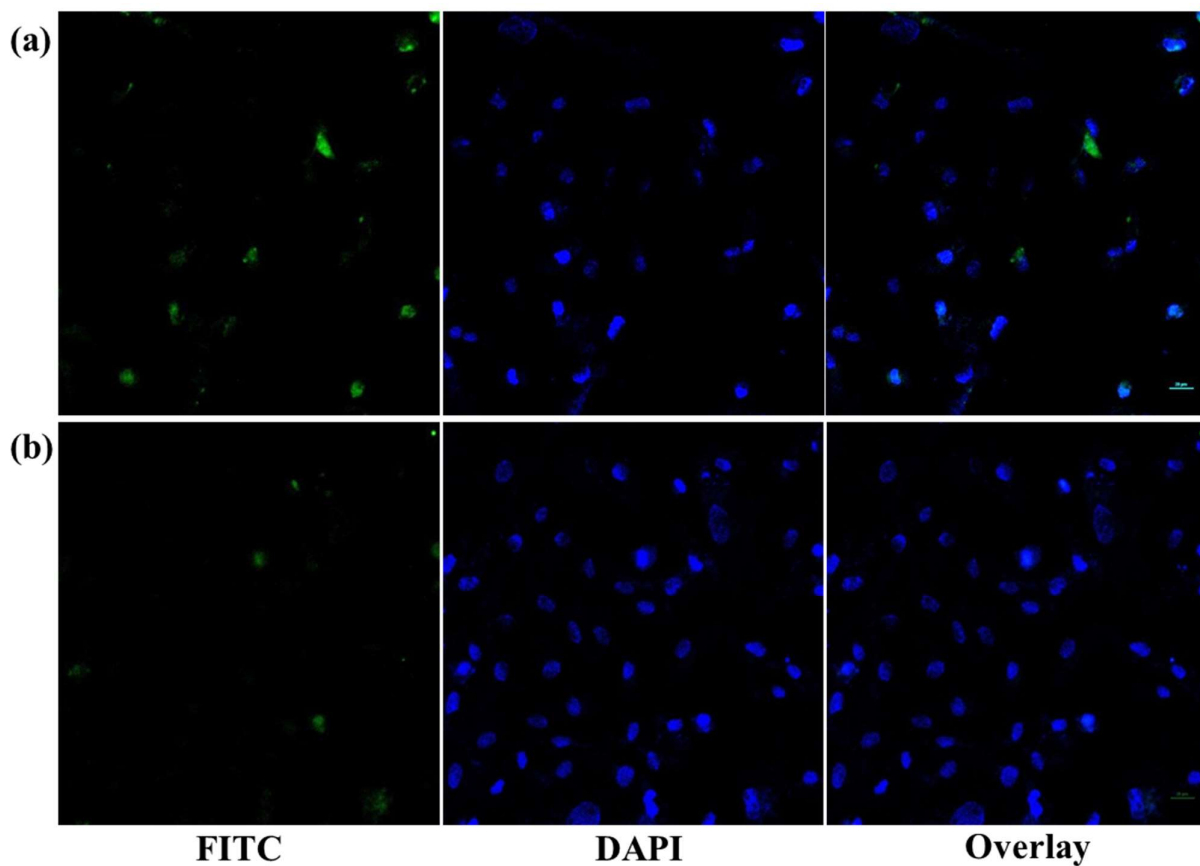
Supplementary Figure 30. Confocal microscopy of the cellular uptake of FITC-labeled Tf-conjugated gold nanospheres in HT29 cells. To clarify endocytosis, uptake studies were done with (a) gold nanospheres coated with transferrin depleted human plasma (10%), (b) gold nanospheres coated with transferrin depleted human serum (50%). Green fluorescence, FITC; blue fluorescence, nuclei stained with DAPI. All pictures are with same magnification and the scale bars represent 20 μm .



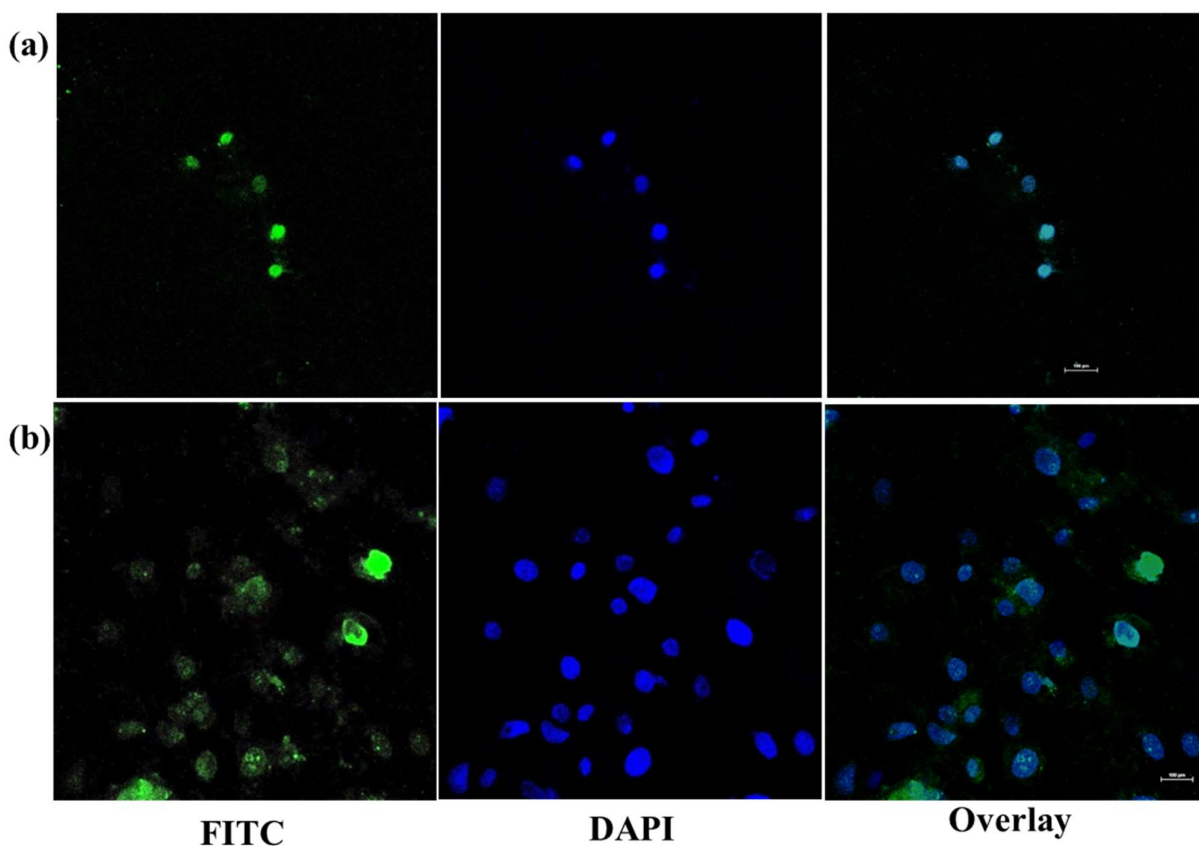
Supplementary Figure 31. Confocal microscopy of the cellular uptake of FITC-labeled Tf-conjugated gold nanospheres in HT29 cells. To clarify endocytosis, uptake studies were done with (a) gold nanospheres coated with Tf excess plasma (10%), (b) gold nanospheres coated with Tf excess plasma (50%). Green fluorescence, FITC; blue fluorescence, nuclei stained with DAPI. All pictures are with same magnification and the scale bars represent 20 μm.



Supplementary Figure 32. Confocal microscopy of the cellular uptake of FITC-labeled Tf-conjugated gold nanospheres in OVCAR3 cells. To clarify endocytosis, uptake studies were done with (a) healthy human plasma coated gold nanospheres (10%), (b) healthy human plasma coated gold nanospheres (50%). Green fluorescence, FITC; blue fluorescence, nuclei stained with DAPI. All pictures are with same magnification and the scale bars represent 20 μm .



Supplementary Figure 33. Confocal microscopy of the cellular uptake of FITC-labeled Tf-conjugated gold nanospheres in OVCAR3 cells. To clarify endocytosis, uptake studies were done with (a) gold nanospheres coated with transferrin depleted human plasma (10%), (b) gold nanospheres coated with transferrin depleted human plasma (50%). Green fluorescence, FITC; blue fluorescence, nuclei stained with DAPI. All pictures are with same magnification and the scale bars represent 20 μm .



Supplementary Figure 34. Confocal microscopy of the cellular uptake of FITC-labeled Tf-conjugated gold nanospheres in OVCAR3 cells. To clarify endocytosis, uptake studies were done with (a) gold nanospheres coated with Tf excess plasma (10%), (b) gold nanospheres coated with Tf excess plasma (50%). Green fluorescence, FITC; blue fluorescence, nuclei stained with DAPI. All pictures are with same magnification and the scale bars represent 20 μm.

Supplemental References

1. Mirsadeghi, S. *et al.* Protein corona composition of gold nanoparticles/nanorods affects amyloid beta fibrillation process. *Nanoscale* **7**, 5004-5013 (2015).
2. Xia, X. *et al.* Quantifying the coverage density of poly (ethylene glycol) chains on the surface of gold nanostructures. *ACS nano* **6**, 512-522 (2011).
3. Choi, C.H.J., Alabi, C.A., Webster, P. & Davis, M.E. Mechanism of active targeting in solid tumors with transferrin-containing gold nanoparticles. *Proceedings of the National Academy of Sciences* **107**, 1235-1240 (2010).
4. Li, J.-L. *et al.* In vitro cancer cell imaging and therapy using transferrin-conjugated gold nanoparticles. *Cancer letters* **274**, 319-326 (2009).
5. Schmid, F.X. Biological macromolecules: UV-visible spectrophotometry. *e LS* (2001).
6. Hu, Y.-J., Liu, Y., Zhang, L.-X., Zhao, R.-M. & Qu, S.-S. Studies of interaction between colchicine and bovine serum albumin by fluorescence quenching method. *Journal of Molecular Structure* **750**, 174-178 (2005).
7. Lu, Y. *et al.* Molecular mechanism of interaction between norfloxacin and trypsin studied by molecular spectroscopy and modeling. *Spectrochimica Acta Part A: Molecular and Biomolecular Spectroscopy* **75**, 261-266 (2010).
8. Zhou, Q. *et al.* Investigation on the interaction between a heterocyclic aminal derivative, SBDC, and human serum albumin. *Colloids and Surfaces B: Biointerfaces* **61**, 75-80 (2008).
9. Gerbanowski, A., Malabat, C., Rabiller, C. & Gueguen, J. Grafting of aliphatic and aromatic probes on rapeseed 2S and 12S proteins: influence on their structural and physicochemical properties. *Journal of agricultural and food chemistry* **47**, 5218-5226 (1999).
10. Zeinabad, H.A. *et al.* Thermodynamic and conformational changes of protein toward interaction with nanoparticles: a spectroscopic overview. *RSC Advances* **6**, 105903-105919 (2016).
11. Rai, A.J. *et al.* HUPO Plasma Proteome Project specimen collection and handling: towards the standardization of parameters for plasma proteome samples. *Proteomics* **5**, 3262-3277 (2005).
12. Elbashir, S.M. *et al.* Duplexes of 21-nucleotide RNAs mediate RNA interference in cultured mammalian cells. *nature* **411**, 494 (2001).